

## OptoSense: Towards Ubiquitous Self-Powered Ambient Light Sensing Surfaces

DINGTIAN ZHANG, Georgia Institute of Technology

JUNG WOOK PARK, Georgia Institute of Technology

YANG ZHANG, Carnegie Mellon University

YUHUI ZHAO, Georgia Institute of Technology

YIYANG WANG, Georgia Institute of Technology

YUNZHI LI, Georgia Institute of Technology

TANVI BHAGWAT, Georgia Institute of Technology

WEN-FANG CHOU, Georgia Institute of Technology

XIAOJIA JIA, Georgia Institute of Technology

BERNARD KIPPELEN, Georgia Institute of Technology

CANEK FUENTES-HERNANDEZ, Georgia Institute of Technology

THAD STARNER, Georgia Institute of Technology

GREGORY D ABOWD, Georgia Institute of Technology

Ubiquitous computing requires robust and sustainable sensing techniques to detect users for explicit and implicit inputs. Existing solutions with cameras can be privacy-invasive. Battery-powered sensors require user maintenance, preventing practical ubiquitous sensor deployment. We present OptoSense, a general-purpose self-powered sensing system which senses ambient light at the surface level of everyday objects as a high-fidelity signal to infer user activities and interactions. To situate the novelty of OptoSense among prior work and highlight the generalizability of the approach, we propose a design framework of ambient light sensing surfaces, enabling implicit activity sensing and explicit interactions in a wide range of use cases with varying sensing dimensions (0D, 1D, 2D), fields of view (wide, narrow), and perspectives (egocentric, allocentric). OptoSense supports this framework through example applications ranging from object use and indoor traffic detection, to liquid sensing and multitouch input. Additionally, the system can achieve high detection accuracy while being self-powered by ambient light. On-going improvements that replace Optosense's silicon-based sensors with organic semiconductors (OSCs) enable devices that are ultra-thin, flexible, and cost effective to scale.

**CCS Concepts:** • Human-centered computing → Ubiquitous and mobile computing; Interaction devices.

---

Authors' addresses: Dingtian Zhang, Georgia Institute of Technology, Atlanta, Georgia, dingtianzhang@gatech.edu; Jung Wook Park, Georgia Institute of Technology, Atlanta, Georgia, jwpark@gatech.edu; Yang Zhang, Carnegie Mellon University, Pittsburgh, Pennsylvania, yang.zhang@cs.cmu.edu; Yuhui Zhao, Georgia Institute of Technology, Atlanta, Georgia, yzhao343@gatech.edu; Yiyang Wang, Georgia Institute of Technology, Atlanta, Georgia, diana.wang@gatech.edu; Yunzhi Li, Georgia Institute of Technology, Atlanta, Georgia, yunzhi@gatech.edu; Tanvi Bhagwat, Georgia Institute of Technology, Atlanta, Georgia, tbhagwat6@gatech.edu; Wen-Fang Chou, Georgia Institute of Technology, Atlanta, Georgia, wfchou@gatech.edu; Xiaoja Jia, Georgia Institute of Technology, Atlanta, Georgia, xjia30@gatech.edu; Bernard Kippelen, Georgia Institute of Technology, Atlanta, Georgia, kippelen@gatech.edu; Canek Fuentes-Hernandez, Georgia Institute of Technology, Atlanta, Georgia, canek@ece.gatech.edu; Thad Starner, Georgia Institute of Technology, Atlanta, Georgia, thad@gatech.edu; Gregory D Abowd, Georgia Institute of Technology, Atlanta, Georgia, abowd@gatech.edu.

---

Permission to make digital or hard copies of all or part of this work for personal or classroom use is granted without fee provided that copies are not made or distributed for profit or commercial advantage and that copies bear this notice and the full citation on the first page. Copyrights for components of this work owned by others than ACM must be honored. Abstracting with credit is permitted. To copy otherwise, or republish, to post on servers or to redistribute to lists, requires prior specific permission and/or a fee. Request permissions from permissions@acm.org.

© 2020 Association for Computing Machinery.

2474-9567/2020/9-ART103 \$15.00

<https://doi.org/10.1145/3411826>

Additional Key Words and Phrases: Ambient light sensing, activity detection, multitouch and hover input, self-powered wireless systems

#### ACM Reference Format:

Dingtian Zhang, Jung Wook Park, Yang Zhang, Yuhui Zhao, Yiyang Wang, Yunzhi Li, Tanvi Bhagwat, Wen-Fang Chou, Xiaojia Jia, Bernard Kippelen, Canek Fuentes-Hernandez, Thad Starner, and Gregory D Abowd. 2020. OptoSense: Towards Ubiquitous Self-Powered Ambient Light Sensing Surfaces. *Proc. ACM Interact. Mob. Wearable Ubiquitous Technol.* 4, 3, Article 103 (September 2020), 27 pages. <https://doi.org/10.1145/3411826>

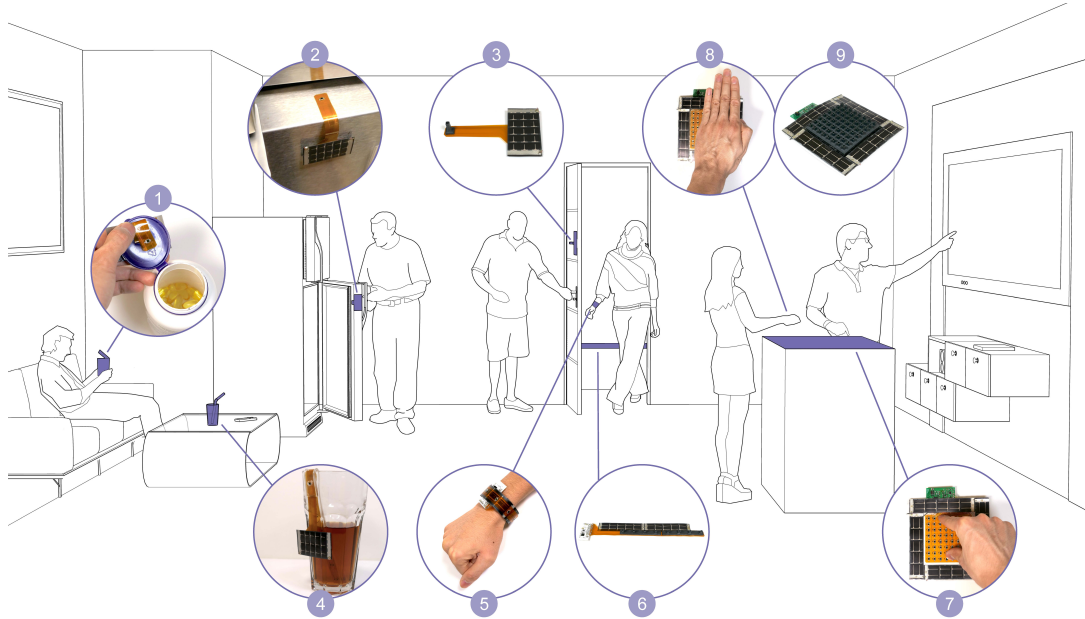


Fig. 1. Application scenarios of OptoSense: (1) Medication reminder. (2) Door open sensing. (3) Presence detection. (4) Liquid sensing. (5) Step counting wristband. (6) Indoor traffic sensing. (7) 2D multitouch input. (8) Hover gesture input. (9) Hover gesture input with extended range.

## 1 INTRODUCTION

Many human activities interfere with ambient light in a predictable and detectable way in that our activities implicitly or explicitly block the paths of ambient light in our environment (Fig. 1). For instance, opening and closing a door, a drawer, or a container implicitly affects the amount of light incident upon inner surfaces of these objects. Similarly, as we walk, our inner arms are periodically blocked from ambient light, and when we take a sip of coffee, the liquid submerges the lowered portion of the inner surface of its container and blocks light on it. This phenomenon also happens during explicit interactions such as touch input; the shadow of the user’s hand gets darker and better defined as it gets closer to a surface, which can be leveraged for touch and hover input.

With OptoSense, we develop a self-powered optical sensing surface to leverage ambient light interference patterns due to human activities as a general-purpose signal at the surface level of everyday objects for activity recognition as well as novel interaction techniques. Through strategic integration with the physical surfaces of everyday objects, OptoSense can capture ambient light signals that are most relevant to the events of interest using

arrays of photodetectors. In comparison to a camera, which is also a general-purpose optical sensing platform, Optosense's ability to capture the most relevant signals means that we can use fewer pixels (as little as one), lower complexity algorithms (such as simple thresholding), and ultra-low-power systems for local computation. OptoSense has four main advantages which make it more practical compared to cameras. First, OptoSense has a **flexible form factor** that allows it to conform to various shapes and geometries of everyday objects and capture field of views (FoVs) that are too large or difficult to access for a conventional camera. Second, the strategic integration and the relatively low spatial resolution of OptoSense decreases the probability of capturing unintended information, better **preserving user privacy**. Third, low power systems can more feasibly achieve **self-sustained operation** through energy harvesting, reducing maintenance efforts as their sheer number increases. Last but not least, the cost of a compact camera is typically higher than a few photodetectors, such that OptoSense is more **cost effective** for scaling to ubiquitous deployment on everyday objects.

OptoSense is inspired by recent work which demonstrated the opportunity to use ambient light sensing to support interactivity with pre-defined gestures on wearable devices or on static surfaces [29, 31, 56, 57]. In comparison, we are particularly interested in generalizing light sensing as a truly “ambient” technology that is not limited to a few niche interactions but can enable an expressive design space once distributed onto surfaces of everyday objects at scale. In this regard, we create a design framework for ambient light sensing surfaces which expands upon previous work by presenting our approach and implementation that uniquely enable a wide range of applications.

Specifically, OptoSense consists of off-the-shelf photodetectors, microcontrollers, and flexible photovoltaic (PV) cells to provide a self-powered ambient light sensing surface. OptoSense uses flexible printed circuits (FPCs) to conform to everyday surfaces, and 3D-printed flexible optical masks to achieve desired fields of view and sensing ranges. In addition to the system, we also present a design space (Fig. 5) based on variations of parameters, including activity type (implicit, explicit), sensing dimensions (0D, 1D, 2D), field of view (wide, narrow), and sensing perspective (egocentric, allocentric), with a comprehensive set of example applications of both previous research and those that are uniquely proposed in this work. Through this design space, we provide design guidelines for OptoSense, hoping to provide further inspirations for future work on ambient light sensing surfaces. Moreover, we demonstrate OptoSense with several representative applications, the evaluation of which indicates that our system is accurate and robust under different lighting conditions.

Finally, we investigate the possibility of replacing silicon-based photodetectors with organic semiconductors (OSC) with much thinner and flexible form factors, and amenability to additive mass manufacturing processes that drive down the cost. With some preliminary results, we demonstrate the feasibility of OSC-based ambient light sensing surfaces that could achieve the above properties, which offer a practical path towards ubiquitous deployment for Internet of Things, smart environments, and ultimately achieving ubiquitous computing.

## 2 RELATED WORK

### 2.1 Distributed Sensing on Everyday Surfaces

Weiser [59] and Ishii [18] have envisioned a world where physical objects and computing are inseparable. As the appearance and functionality of electronics and everyday objects are converging, we see more research exploiting the surfaces of objects to mediate our direct manipulation of the objects.

Prior work has demonstrated sensing surfaces by utilizing patterned conductive materials. For instance, inkjet printing has been used to produce touch sensing circuits on paper with a home printer [22]. Wall++ [66] applied conductive paints to walls to enable room-scale capacitive and electromagnetic sensing. Touch sensing has also been achieved by Electric Field Tomography on conductive materials which can be easily coated onto everyday objects [63, 65]. Jacquard [39] and I/O Braid [38] employed conductive yarns to fabricate interactive textiles as wearable interfaces. Duoskin [21] explored temporary tattoos with conductive materials that support touch

interaction on human skin. Objectskin [11] demonstrated hydroprinting conductive materials onto rigid and flexible everyday objects. It is also possible to leverage other materials and physical phenomena for interactive sensing, such as piezoelectric films for touch sensing [41], optical fibers for grasp sensing [60], and triboelectric cord for self-deformation sensing [45]. Enabling a wide range of form factors and use cases, these technologies have illuminated a promising path of distributed sensing on everyday surfaces by leveraging the ease of fabrication and deployment of conductive materials, using additive technologies such as printing or painting on a variety of substrates. Optosense's increased sensing range extends previous work on touching and hovering to allow monitoring of implicit activities. In addition, Optosense's low power budget allows large-scale applications and deployments, and its sensing is not affected by being mounted on metallic surfaces such as refrigerators.

## 2.2 Self-Sustained Sensing

There is an increasing body of research on self-sustained ubiquitous sensing by energy harvested from the environment, which is also relevant to our system. Many energy sources have been explored, including solar [29, 31, 36, 49, 51, 55, 56] and RF backscattering [10, 26, 30, 35, 40, 43, 50]. Other less common energy sources include thermal [67], hydraulic [8], kinetic [46], triboelectric [2, 45], and combining multiple energy types for a coverage of wider range of activities [64].

Sunlight and artificial light are among the most common energy sources for self-sustained systems due to their pervasiveness in our living environments and that they can be harvested with photovoltaic (PV) cells. Compared to commonly used rigid crystalline silicon (c-Si) PV cells, amorphous silicon (a-Si) PVs can be flexible and can conform to everyday objects. Under indoor illumination conditions, the power conversion efficiency (PCE) of c-Si and a-Si PV cells is typically below 10% (with a theoretical maximum PCE of 22%) because they are optimized to operate at high irradiance conditions [32]. However, the PCE of emerging flexible PV technologies such as those based on perovskite and organic semiconductors have improved significantly, with values as high as 36% (perovskite PV) and 27.8% (OPV) under indoor illumination conditions (white LED) [6]. These PV technologies could provide at least  $250 \mu\text{W}/\text{cm}^2$  of electrical power under indoor illumination where the energy density varies from  $0.1 - 1 \text{ mW}/\text{cm}^2$  [9]. Although we demonstrate OptoSense with commodity a-Si PV cells, emerging flexible PV cells will enable significant reductions of the PV footprint.

It is also possible to use multiple silicon photodiodes to increase the total effective area to harvest energy [29, 36, 51]. With a smaller footprint, photodiodes can be mounted on flexible substrates to achieve certain level of flexibility. Despite its strength, the number of photodiodes needed to provide enough energy for functionalities such as computation and communication is quite high. Additionally, the dual use of photodiodes for sensing and energy harvesting often adds to the computational and circuit complexity. Both lead to an increased cost of the system. In this paper, we use separate energy harvesting and optical sensing for the benefit of power, cost, and design complexity.

## 2.3 Optical Sensing

More relevant to OptoSense are prior approaches which also leverage optical sensing as a general-purpose approach for sensing human activities and interactions. The field of human-computer interaction (HCI) has seen a long history of coupling optical sensors with other human-computer interfaces to enhance their input modalities. Previous work has leveraged infrared (IR) receivers (e.g., photodiodes, phototransistors) and emitters (e.g., LEDs) in concert with a wide range of devices, such as embedded beneath a display [13, 14], on the bezel of a display [1, 33], on a keyboard [12, 52], on the side of a mobile device [7], and on a wearable device [24]. These sensors capture proximity information of a user's finger, hand, and arm to enable additional touch, hover, and gesture input. These examples leveraged light emitters as an active signal source which made them less affected by ambient light, yet often more power intensive than passive sensing approaches.

The closest to our approach are prior systems that also utilize ambient light for interactions. For instance, using exclusively ambient light, Li et al. [29] demonstrated self-powered optical sensing of discrete tap and mid-air swipe gestures with a 1D photodetector array on a pair of smart glasses or a watch. SolarGest [31] presented battery-free gesture recognition using a single transparent organic solar panel on a smartwatch. Varshney et al. [56] showed a similar battery-free solar-cell-based hand gesture recognition system with analog backscatter communication. However, prior work focused on near-surface interactions with limited sensing dimensions (0D and 1D) and thus missed the applications that require richer expressiveness of input and longer sensing range. In comparison, OptoSense extends beyond prior work by enabling continuous multitouch tracking and mid-air swipe gestures on 2D surfaces of everyday objects, unlocking the potential of numerous applications. Moreover, as we will discuss in greater detail, the system can be generalized to recognize user activities, which uniquely enables a wide range of smart home and IoT applications.

It is also possible to deploy optical sensors in a room to sense implicit human activities at a room scale. Li et al. [27, 28] deployed frequency-modulated LEDs on the ceiling and photodiodes on the floor to extract a real-time user skeleton from light blocking information. Without modifications to lighting infrastructure, Venkatnarayan and Shahzad [57] demonstrated ambient light whole-body gesture recognition using light sensors on the floor and a PC running machine learning algorithms. We extend ambient-light-based activity sensing by investigating three sensing dimensions (0D, 1D, and 2D) and two sensing perspectives (egocentric and allocentric) combined with a self-powered system for on-board local computation and wireless communication.

### 3 PRINCIPLES OF AMBIENT LIGHT SENSING

OptoSense senses changes in the intensity of ambient light incident upon a surface to reveal meaningful information related to object or human behaviors. In a typical lighting environment, light impinges a photodetector's surface from all directions within its field of view (FoV): direct light from point light sources and diffuse light from surface reflections. An object within the photodetector's FoV will change the photodetector's total incident light intensity depending upon the object's opacity, the distribution of ambient light, and the solid angle subtended by the object, as seen from the photodetector. To understand the relationship between these factors, first consider the optical power received by a bare unblocked photodetector of area  $A_d$ :

$$\Phi_d = \int_0^{2\pi} d\psi \int_0^{\Theta} A_d L_s(\theta, \psi) \sin(\theta) \cos(\theta) d\theta \quad (1)$$

where  $L_s(\theta, \psi)$  is the angular-dependent radiance of the scene,  $\psi$  is the azimuthal angle,  $\theta$  the polar angle, and  $\Theta$  is the chief ray angle which defines the field of view (FoV). In a scene, the illumination conditions can produce a radiance distribution that can be quite complex, resulting from a combination of point or small-area sources (e.g., the sun, a light bulb, stars), specular reflections (e.g., from metals), and diffuse sources (e.g., light reflected from the ceiling, the sky, etc.). For simplicity but without losing generality, we assume that  $L(\theta, \psi) = L$ . That is, the ambient light illumination is uniform and independent of the angle (i.e., the Lambertian approximation). The chief ray angle  $\Theta$  is defined as the ray that starts at the edge of a light source, passes through the center of the aperture stop of an optical system and ends at the edge of the field stop (here the edge of the photodetector). Note that  $\Theta$  can be a function of  $\psi$  in the absence of radial symmetry. If a photodetector is used without a limiting aperture (i.e., the aperture stop is also the field stop), the effective chief ray angle will be defined by its angular-dependent responsivity, or  $\Theta_d$  in this case. Therefore, the total optical power of the scene on a bare photodetector can be simplified as:

$$\Phi_{scene} = \pi A_d L \sin^2(\Theta_d) \quad (2)$$

If an object of opacity  $\kappa$  blocks light from the scene within a polar angle  $\Theta_{obj}$ , the optical power onto the photodetector will be reduced by  $\Phi_{obj} = \kappa\pi A_d L \sin^2(\Theta_{obj})$ . As shown in Fig. 2 (a), the object being detected is represented by a disk of radius  $r$  and size  $\pi r^2$ , located directly above the photodetector at distance  $d$ , such that the ratio of optical power being blocked can be described:

$$\phi = \frac{\Phi_{obj}}{\Phi_{scene}} = \frac{\kappa \sin^2(\Theta_{obj})}{\sin^2(\Theta_d)} = \frac{\kappa r^2}{(r^2 + d^2) \sin^2(\Theta_d)} \quad (3)$$

We can see that the ratio  $\phi$  is approximately proportional to  $d^{-2}$ . As  $d$  increases,  $\phi$  decreases rapidly to below the detection threshold, resulting in a relatively short sensing range. For applications that require a longer sensing distance beyond a few inches above the surface, we can restrict the FoV of a photodetector with an aperture stop—an optical mask with opaque and nonreflective light tunnels of controlled height ( $H$ ) and width ( $W$ ) on top of individual photodetectors, similar to the approach followed by Immega et al. [16]. Ambient light coming from off angles will be blocked by the tunnels while only light within the reduced FoV with chief ray angle  $\Theta_{tunnel}$  can reach the photodetector. This situation is preferable to using a lens with a fixed focal length since the aspect ratio ( $H/W$ ) of the light tube can easily be modified to control the FoV. Fig. 2 (b) illustrates the effect of the optical mask on a photodetector. The ratio of optical power being blocked can be amplified as:

$$\phi = \frac{\kappa \sin^2(\Theta_{obj})}{\sin^2(\Theta_{tunnel})} = \frac{\kappa r^2 (W^2 + 4H^2)}{(r^2 + d^2) W^2} \quad (4)$$

The ambient light blocking ratio  $\phi$  in (3) or (4) is the basis of ambient light sensing, which is affected by both intrinsic factors (FoV of the photodetector) as well as extrinsic factors (object size, distance, and opacity). For a single photodetector, the closer  $\phi$  is to 1, the more confident we can be about the presence of an object. Derivatives of  $\phi$  along the time axis can reveal temporal patterns, and derivatives across multiple photodetectors of various form factors can subtract additive noise or extract spatial features of the signal. Details of applying the ambient light sensing principles will be discussed in the following sections as we describe the design and applications of OptoSense.

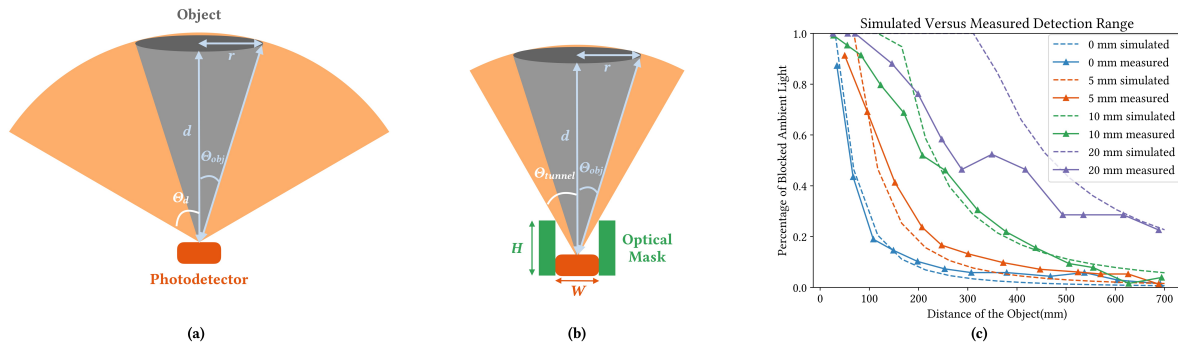


Fig. 2. Modeling of sensing range of photodetectors (a) without and (b) with an optical mask. (c) The numerical simulation versus the actual measurements of the detection range for light tunnels with different heights (mm).

#### 4 OPTOSENSE SYSTEM

In this section, we discuss the design and implementation of OptoSense as a general-purpose self-powered ambient light sensing system, including analytical and empirical data of its sensing and power requirements.

OptoSense supports a variety of sensing surface designs, all of which can operate autonomously with harvested energy. There are two main components of OptoSense: 1) a flexible imaging surface for sensing and energy harvesting; and 2) a control circuit for power management, computation, and communication. Using off-the-shelf silicon-based photodetectors, flexible PV cells and substrates, OptoSense implements the imaging surface with three configurations (i.e., 0D, 1D, and 2D) and can conform to complex everyday surfaces with varying sizes. The custom control circuit is built around low-power components including a microcontroller, multiplexers, and a power management integrated circuit (IC) to perform sensing and computation on board, and send results wirelessly to smart devices (e.g., phones, smart TVs, smart home speakers) via Bluetooth Low Energy (BLE). The system design aims to show a path towards ubiquitous ambient light sensing surfaces that use emerging technologies of flexible optoelectronic components.

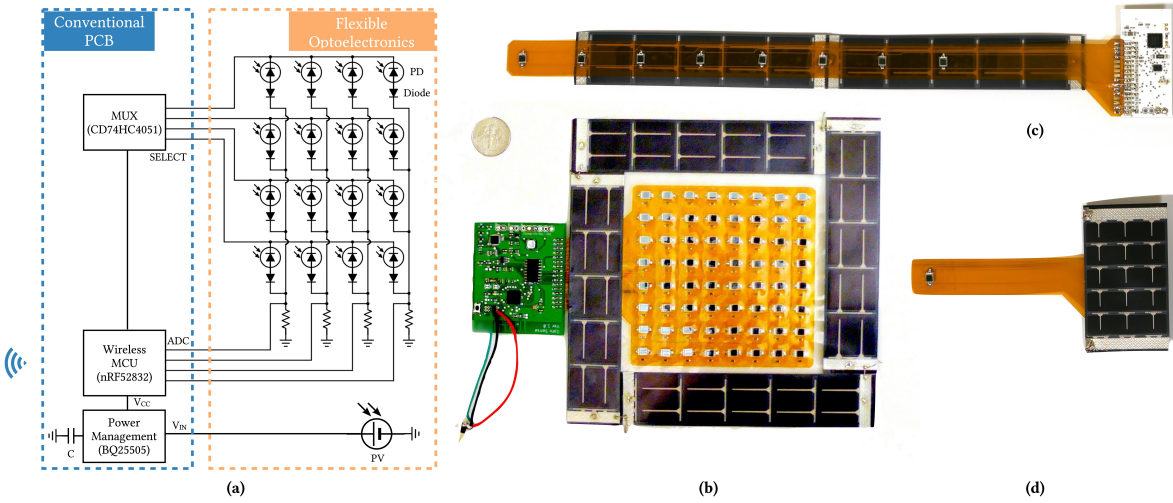


Fig. 3. OptoSense hardware design: (a) Schematic. (b) Implementations of OptoSense systems using 0D, (c) 1D, and (d) 2D photodetector arrays.

#### 4.1 Flexible Imaging Surface for Sensing and Energy Harvesting

The imaging surface senses with 0D, 1D, and 2D arrays of photodetectors. OptoSense has a parallel connection for 1D and a passive imaging array with a row/column polling mechanism for 2D, where each pixel is comprised of a photodiode and a rectifying diode (to prevent crosstalk). Compared to an active array which uses a transistor instead of a diode, passive designs require fewer interconnects and less power for switching on/off a pixel. The rows are connected to a multiplexer on the control circuit, and columns are connected to the analog-digital converters (ADCs) of the microcontroller and load resistors for converting photocurrent to voltages, as shown in Fig. 3 (a). Note that this interconnection design can also scale with the number of pixels and be applied to emerging optoelectronic devices and their fabrication processes.

For the actual prototypes, we implemented the 0D (single pixel), 1D ( $1 \times 8$  array), and 2D ( $8 \times 8$  array) sensors on a polyimide FPC. Each pixel has a PIN photodiode (BPW34). For 2D configurations, a small signal Schottky diode (BAS40-02V-V-G) is used per pixel. The photodiodes operate in reverse bias mode for linear response to light intensity and greater sensing range (versus zero bias mode). The load resistors can be adjusted to achieve a desired dynamic range. Using 12-bit ADCs, a 10k resistor can measure indoor lighting intensity up to 4k lux with

a step of 1.5 lux; a 1k resistor can be used for outdoor scenarios (100k lux) but with a lower resolution of 10 lux steps.

For energy harvesting, we use flexible a-Si PVs (PowerFilm MP3-25 & SP3-37) with a PCE of around 5% in parallel connections. We placed the flexible PV cells alongside, or even underneath, the semi-transparent polyimide substrate for energy harvesting from ambient light.

#### 4.2 Optical Mask For Sensing Range Tuning

To extend the sensing range of the photodiodes, we 3D printed optical masks for 0D, 1D, and 2D configurations (Fig. 4) using a Form 3 printer and the Flexible V2 photopolymer resin from Formlabs. Once cured, the material becomes opaque, dark colored, rubber-like, and flexible upon bending. We applied the optical mask onto the flexible sensing surfaces of OptoSense using laser-cut adhesive transfer tapes. The optical mask is designed to maximally preserve the flexible form factor and cost effectiveness of OptoSense.

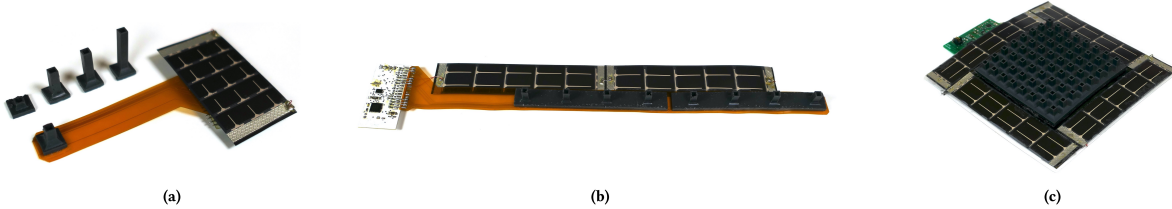


Fig. 4. 3D-printed flexible optical masks showing 10 mm integrated light tunnels. (a) 0D OptoSense with replaceable 5, 10, 15, 20, and 25 mm tunnels. (b) 1D OptoSense. (c) 2D OptoSense.

The FoV of the bare photodiode we use is about  $120^\circ$ ; beyond this angular range the responsivity falls off rapidly due to reflection losses (Fig. 2 (a)). The active area of the photodiode is around  $2.65 \text{ mm} \times 2.65 \text{ mm}$ , such that  $W = 2.65 \text{ mm}$ . We varied the height of the light tunnel  $H$  to be  $\{5, 10, 20\} \text{ mm}$  (Fig. 2 (b)). Fig. 2 (c) shows a comparison of experimental results and numerical simulation of the power measured by a photodetector in response to a laser-cut plywood disk of 50 mm radius, placed at various distances from the photodetector against a near hemispheric background constructed with white cardboards. The disk is used to represent objects of similar shape and size such as a human hand. Despite some misalignment at close distances due to ambient light reflections from the object, general agreement between simulations and measurements validates that the FoV of the photodetector controls its sensing range. The sensing range can be defined by an arbitrary threshold of  $\phi$ , below which the object is considered as detected. For  $\phi = 40\%$ , the sensing range increases from  $d = 70 \text{ mm}$  with the bare photodetector to  $d = 500 \text{ mm}$  with the photodetector enclosed inside a light tunnel of  $H = 20 \text{ mm}$ .

#### 4.3 Control Circuit for Power Management, Computation, and Communication

At the core of the control circuit sits a low-power microcontroller (Nordic nRF52832 using an ARM Cortex-M4 CPU), which controls a low-power analog multiplexer (TI cd74hc4051) to switch the rows of the 2D photodiode array to apply a reverse-bias voltage, samples from each column sequentially with ADCs, processes the sensor data on-board to extract input information, and communicates wirelessly via BLE.

As lighting conditions vary and fluctuate, we use a low-power boost converter (TI bq25505) and a thin 3.7 V 105 mAh Lithium Ion Polymer battery to store surplus energy from the photovoltaics to serve as a backup power source when ambient light is low.

#### 4.4 System Operation and Energy Consumption

The microcontroller duty cycles between sleep and active modes to balance power consumption and fast responses to interactions. Power management is set to always ON to regulate and store the energy harvested from the PVs. Within each cycle, the system goes to sleep with the real time clock (RTC) and memory retention on; RTC is set at fixed intervals to wake up the system to complete the tasks of sensing, processing, and communication. We set the operating frequency to 10 Hz for motion and input sensing applications, and 2 Hz for state detection applications where real-time responses are not critical. We measured the power consumption of 0D, 1D, and 2D OptoSense using the Nordic Power Profiler Kit, averaged for five testing rounds, as shown in Table 1.

Table 1. Power consumption of 0D, 1D (1 × 8 array), and 2D (8 × 8 array) OptoSense ( $\mu\text{W}$ )

Activity	0D (2 Hz)	1D (10 Hz)	2D (10 Hz)
Sleep (w/ RTC and memory retention)	6.9	6.9	6.9
Sensor measurement	1.8	11.7	92.1
Local computation	0.9	9	57
BLE transmission (0dBm)	37	152	154
Total	46.6	179.6	310

Comparing 1D and 2D OptoSense operating at the same frequency (10 Hz), the power consumption of sleep and BLE transmission remains largely the same while the power consumption of sensor measurement and computation increases with the number of pixels, such that the area of energy harvesting PV cells should also increase in proportion to provide extra energy. Note that the power consumption of BLE transmission, as the most power hungry activity, is optimized by performing local computation and communicating the end results only. Communicating raw data directly, especially for 2D (8×8 array) OptoSense, will significantly increase the communication and total energy consumption.

#### 4.5 Energy Harvesting

We investigated the amount of energy the system can harvest in six typical lighting conditions recommended by the IES Handbook [4], as shown in Table 2. We also adopted these illumination levels in our evaluation to best reflect realistic scenarios in everyday settings. For accurate measurements, we placed the solar panel of our system underneath a incandescent light source in a light-blocking enclosure and measured the ground-truth illumination with a digital light meter.

Table 2. Output of the energy harvesting circuit (bq25505) in various lighting conditions

Condition	Illumination (lux)	Power ( $\mu\text{W}$ )	
		PowerFilm SP3-37 64.0 x 36.8 (mm)	PowerFilm MP3-25 114.0 x 24.0 (mm)
Easy office work, classes	250	28.8	34.5
Normal office work	500	69.7	121.8
Mechanical workshops	750	133.4	250.9
Normal drawing work	1000	214.7	411.3
Detail mechanical work	2000	866.1	824.1
Performance of visual tasks	5000	2048.0	3082.3

According to the measurements (Table 2), 2D ( $8 \times 8$  array) OptoSense can operate indefinitely at 500 lux ambient light intensity with 3 pieces of MP3-25 PV ( $82.1 \text{ cm}^2$ ) without an additional backup battery. For 0D or 1D systems, 1 or 2 pieces of PV cells are enough to power under the same ambient light condition. The use of a small battery can help store the surplus energy when the ambient light is abundant so that it can be supplied later in dim conditions. Note that at 500 lux the power density generated by the SP3-37 PV and MP3-25 PV was below  $4.45 \mu\text{W/cm}^2$  corresponding to a PCE of 3.4%. State-of-the-art OPVs and perovskite PVs have reached PCE above 25% [32] which correspond to  $32 \mu\text{W/cm}^2$  under the same illumination conditions. This advancement means that 2D OptoSense more realistically will only require PV cells with an area of around  $8 \text{ cm}^2$  to operate continuously. Emerging flexible PV with high PCE values will enable one order of magnitude reduction over these commodity a-Si PV cells, such that the PV footprint will be less of a concern.

OptoSense's energy harvesting significantly improves the utility of the sensor. For example, relying on the the 3.7 V 105 mAh battery ( $2.8 \times 16 \times 37 \text{ mm}$ ) alone only lasts for 6.0 weeks of continuous usage (to the maximum 80% battery depletion) for the 2D OptoSense without harvesting energy from ambient light. With large-scale deployment onto surfaces of everyday objects, self-sustained operation is necessary to free the user from constant maintenance efforts of charging or replacing batteries. Another potential advantage of energy harvesting is a reduction in battery waste. The battery in our circuit can be replaced with a supercapacitor to maintain the circuit during times of low light.

## 5 DESIGN FRAMEWORK OF OPTOSENSE

In this section we discuss the design framework of self-powered ambient light sensing. We first describe the parameters that define the design space followed by design guidelines and recommendations. This design space is both explanatory and generative. Our goal is to show how past work and OptoSense fit into this design space and how it serves as an inspiration for new designs of self-powered ambient light sensing surfaces.

### 5.1 Parameters

We first list the important parameters from both optoelectronic and perceptual perspectives to consider when designing OptoSense. These parameters listed below, originating from optical sensing or general HCI, reflect decisions made in previous work and together span the design space of ambient light sensing surfaces.

- **Activity type:** OptoSense supports both **explicit** and **implicit** activities, i.e., activities performed by the user with either the primary intention of interacting with the computing system or not [44]. OptoSense can be used as an input device supporting **explicit** interactions such as touch, hover, or wave [29, 31, 56]. Integrated with everyday objects, OptoSense can also detect ambient light interference patterns, such as walking or jumping [57, 62], as byproducts of daily **implicit** activities without altering user behavior or attention.
- **Sensing dimension:** The choice of using **0D**, **1D**, and **2D** layouts depends on the desired sensing granularity and spatial resolution of activities. For activities that only need to be sensed if or when it happens, the **0D** layout can function as a button [31, 56], or it can detect the state of objects such as a door or a pill bottle. For activities where we are interested in knowing position, direction, speed, and dynamic patterns along only one primary axis, the **1D** layout can be used. Such examples include an interactive slider [29], counting steps as we walk, sensing traffic flow in a hallway, or detecting the liquid type and volume in a container. For activities associated with size, shape, and motion information that span across two axes, the **2D** layout can be used. Such examples include touch tracking, hand gestures, body postures [57], indoor locations [62], and other everyday activities.
- **Field of view and sensing range:** The choice of using the **wide** or **narrow** FoV depends on the desired sensing range. Bare photodetectors with **wide** FoVs are suitable for sensing contact or near-surface (<

50mm) activities such as touch and hover [29, 31, 56], and ambient light illumination [62] in general. **Narrow** FoVs can be achieved with optical masks to extend the sensing range for hand ( $> 0.2$  m) and whole body ( $> 1$  m) activities. Adding to the benefit of low sensing granularity, OptoSense can also better protect user privacy by confining sensing within a desired proximity and locality.

- **Sensing perspective:** OptoSense has tremendous freedom of deployment on various everyday objects to sense not only changes in the environment but also the changes of the object itself in relation to the environment. We recognize the difference in sensing perspective as **egocentric** or **allocentric**, i.e., if the frame-of-reference is located within or external to the perceiver (sensing system) [23]. In a **egocentric** perspective, OptoSense uses its host object as the frame-of-reference and observes activities in its own coordinates. Typically the sensors are deployed on stationary surfaces such as walls, floors [57], desks, and electric appliances to pick up ambient light interference to sense user activities at those particular locations. In an **allocentric** perspective, the frame-of-reference is within the environment, and OptoSense senses activities of the object in world coordinates. Typically the sensors are deployed on mobile objects such as the human body [62], doors, drawers or book pages, and they use motion-induced ambient light changes to infer activities about those objects themselves. Note that how to define the sensing perspective is within the context of the activity; a light-sensing wristband is considered egocentric when it is used as a touch or hover input device [29, 31], but it is allocentric when used to detect walking activity from swinging arms.

## 5.2 Design Space

Once we have the parameters, we can now draw a design space for OptoSense. Following the decisions made on each parameter, we divide the designs into  $2 \times 3 \times 2 \times 2 = 24$  categories, and within each category there is a rich set of applications based on small variations of use cases, locations, form factors, and beyond. The representative applications listed in Fig. 5, which are by no means exhaustive, demonstrate the promise of OptoSense.

In the design space, applications demonstrated in past research are predominately in the set of {0D/1D, explicit interactions} and {2D, implicit activities}, all having wide FoVs and mostly egocentric perspective. We pick a few applications that are diverse and unique to our work for evaluation (highlighted in Fig. 5), described in detail in the following implicit and explicit application sections. We also make a few suggestions of possible use cases of OptoSense in potential applications. Occupancy detection from blocking of ambient light can be implemented on a seat, at a parking space, or around an office desk; position and activity information can be sensed from a door, a wall, or a ceiling. As a wearable, OptoSense can be placed on the head, neck, shoulder, wrist, and foot for activity sensing, position tracking, or gesture input. Placed on an object, OptoSense can sense flipping, touching, hovering, opening, moving, shaking, and other manipulations using ambient light. Many of the listed applications are set in indoor scenarios due to the fact that a great variety of everyday surfaces and objects with which we interact belong indoors. However, OptoSense can be used for outdoor applications such as sensing walking activity, plant sunlight exposure for precision farming, or wild animal and livestock activity monitoring, all self-powered by abundant sunlight. All of these applications would benefit from the cost, power, form factor, and privacy implications of OptoSense.

## 5.3 Design Guidelines of OptoSense

Given the capabilities and design space of OptoSense, here we list a few application design guidelines:

- **Bring sensors closer to activities:** Unlike cameras, conformal form factors allow OptoSense to be tightly integrated with physical objects and share many properties such as orientation and motion. Bringing OptoSense closer to its target activity (e.g., put inside a drawer for opening detection) helps to obtain high fidelity signals with low resolution sensors and low complexity algorithms.

Activity Type	Sensing Dimension	Field of View	Sensing Perspective	Application
Implicit	0D	Wide	Egocentric	Agriculture sunlight meter, seat/parking occupancy sensor
			Allocentric	Object open/close detection (Section 6.1)
		Narrow	Egocentric	Presence detection (Section 6.2)
			Allocentric	On-glasses head tracking
	1D	Wide	Egocentric	Liquid type/level (Section 6.3), desk occupancy sensor
			Allocentric	Walking activity (Section 6.4), animal activity sensing collar
		Narrow	Egocentric	Indoor traffic sensing (Section 6.5)
			Allocentric	—
	2D	Wide	Egocentric	Full body gesture recognition [57]
			Allocentric	Object/wearable light-based indoor positioning [62]
		Narrow	Egocentric	Indoor occupancy/location/activity monitoring
			Allocentric	—
Explicit	0D	Wide	Egocentric	Button, 0D touch/hover input [31, 56]
			Allocentric	Interactive flip cards
		Narrow	Egocentric	—
			Allocentric	Screen-based pointer
	1D	Wide	Egocentric	Slider, 1D touch/hover input [29]
			Allocentric	Dancing/cheering smart bracelet
		Narrow	Egocentric	1D hover input at extended range
			Allocentric	—
	2D	Wide	Egocentric	Trackpad, 2D touch/hover input (Section 7.1 & 7.2)
			Allocentric	Motion tracking game controller
		Narrow	Egocentric	2D hover input at extended range (Section 7.3)
			Allocentric	—

Fig. 5. Design space of OptoSense showing example applications including previous work (shaded in dark gray) based on the decisions of each parameter: activity type, sensing dimension, FoV, and sensing perspective. We show all possible combinations to encourage more applications to fill the space.

- **Bring activities (optically) closer to sensors:** In situations where OptoSense cannot be physically close enough to its target activity (e.g., indoor traffic sensing), optical masks can “bridge the gap” optically. In doing so one must also consider the trade-offs such as a more obtrusive form factor as the tunnel height increases. Additionally, a narrow FoV means a smaller observation area and susceptibility to artifacts, such that a more uniform and stable background is preferred to an uneven or noisy ambient light background.
- **Bring photovoltaics closer to light:** Leveraging the flexible form factor of OptoSense, PV cells can be positioned or oriented differently from sensors to maximize ambient light exposure. Examples include the edge and front of a door, inside and outside of a container, dorsal and ventral side of an arm, etc.

## 6 IMPLICIT ACTIVITY SENSING APPLICATIONS

In this section, we demonstrate the use of OptoSense for everyday activity sensing through the detection of object open versus closed states, human presence, liquid properties, walking activity, and indoor traffic. For each sensing modality, we describe the detection algorithm, evaluation procedure, and results. Note that all detection is achieved with low-complexity rule-based algorithms designed for OptoSense’s low-power microcontroller.

## 6.1 Open Versus Closed State Detection

Our **0D** sensor with a **wide** FoV can be deployed on doors, drawers, closets, cupboards, mailboxes, fridges, pill bottles, etc., where opening those objects results in exposure to light, and closing blocks the light from an **allocentric** perspective. We choose the door and pill bottle as two examples of different scales. Albeit simple, the two examples here show that ambient light as a general-purpose signal can be sensed with high fidelity by a low-power photodetector strategically integrated with surfaces of everyday objects.

For door state detection, we placed the 0D OptoSense prototype on the edge of a door, with the photovoltaic facing outside. For pill bottle state detection, we placed the 0D OptoSense prototype on the inside of the flip top cap of a commodity pill bottle, with the photovoltaic wrapped around to the top of the cap. Fig. 6 (a) (c) shows the setup of both experiments, where photovoltaics could harvest energy from ambient light regardless of the open versus closed states. We set the ambient light intensity at three levels: 250 lux, 500 lux, and 750 lux. Note that these conditions were selected based on previous research on indoor illumination levels and human activities in indoor illumination [4, 15, 34]. Under each lighting condition we repeatedly opened and closed the door or the pill bottle 50 times to test our detection threshold.

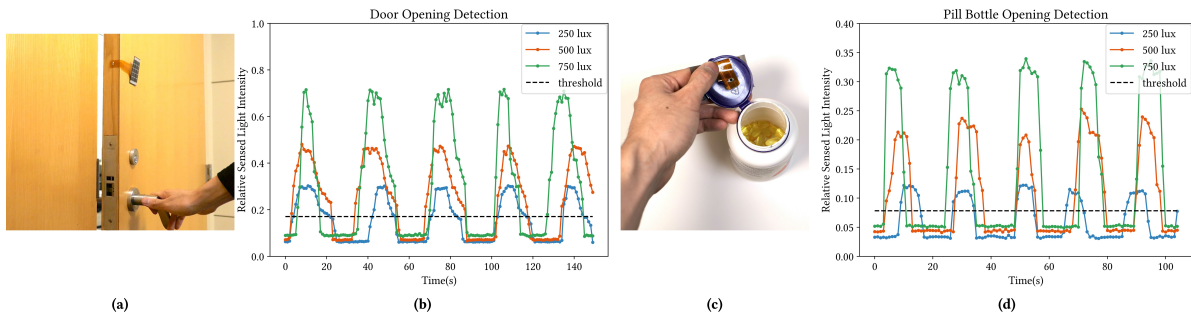


Fig. 6. (a) 0D OptoSense prototype attached to an office door. (c) A pill bottle's cap has the 0D OptoSense prototype attached. (b) Sensed light intensity at door and (d) pill bottle at three different ambient lighting levels, indicating a clear threshold for distinguishing open (above the threshold) and closed (below the threshold).

As shown in Fig. 6 (b) (d), the open and closed states can be easily distinguished across all ambient light levels. We converted the sensor readings to relative light intensity by dividing over the maximum value when the sensor was saturated. As expected, the ambient light level greatly affects the open state sensor reading, and the closed state remains almost unchanged. We achieved 100% detection accuracy of door and pill bottle opening events with thresholds of 0.17 and 0.08, respectively.

## 6.2 Presence Detection

Our **0D** sensor with a **narrow** FoV can be used to detect human presence in an **egocentric** perspective within meters, since the human body blocks a much larger area of ambient light than a hand as seen from a photodetector. The application we developed is to detect a human approaching a door or a corner and show alerts (e.g., with LED lights or a display) on the other side for collision avoidance. The sensor can be easily attached to surfaces and aimed towards incoming traffic. Our algorithm is based on the ambient light blocking ratio  $\phi$  by a human body against the illumination background. Compared to other types of sensing such as a proximity sensor or a camera, our approach is passive, low-power, and privacy-preserving.

We evaluated the application on 10 participants (8 male, 2 female) in lab. We instrumented 0D OptoSense with an optical mask of 10 mm light tunnels on a door at the height of 1 m. The door faced a hallway of two-way

traffic with 250 lux ambient light illumination. For consistency, all prototypes (0D, 1D, 2D) with the optical masks were evaluated under the same level of ambient light (250 lux) to provide a baseline of performance for brighter ambient illuminated conditions. Each of the 10 participants was instructed to walk towards the door until their presence was detected by the sensor, with a detection threshold set to  $\phi = 0.2$ .

Fig. 13 (a) shows our experimental setup and the maximum distance at which the presence was detected for each of the participants averaged over five trials. As a result, we achieved an average detection range of 1.39 m ( $SD = 0.324$  m), with a maximum of 1.89 m and a minimum of 0.92 m, which should be far enough to alert the other side to avoid collision. We did not observe false positives when no human participants were within proximity of the sensor. We observed that the distance of presence detection was affected by the body frame of the participant as well as the color of their clothes. Participants with larger frames wearing darker-colored clothes were detected at greater distances compared to those with smaller frames wearing light-colored clothes, due to the amount of ambient light blocked by objects of different sizes and light absorption.

### 6.3 Liquid Sensing

We waterproofed **1D** OptoSense with **wide** FoVs in a transparent polymer (PDMS) in order to explore whether it could identify the type and level of liquid in an open container from an **egocentric** perspective (see Fig. 7). By measuring the ambient light occlusion along one dimension, we can quantify and identify translucent or opaque content in an open or transparent container. Specifically, when liquid is poured into a container, pixels submerged below or close to the liquid level will receive less ambient light compared to the higher pixels (we always keep the highest pixel above the liquid level to capture a reference value of the ambient light). The gradients between pixels can be used to infer the liquid type and level. Compared to other sensing modalities that only detect liquid level (e.g., capacitive, resistive) or type (e.g., fiber optic, ion sensor), ambient light sensing is feasible for both of the tasks using simple rule-based methods that run on a low-power microprocessor without sophisticated features or machine learning.

Our algorithms for liquid type and level detection work as follows:

- **Liquid Type Detection:** From our observation, the ratio of the light intensity at the bottom pixel (when submerged in the liquid) to the top pixel (always above the liquid level) is a reliable indicator of the liquid type. The less transparent the liquid, the smaller the ratio. We use that ratio to classify the liquid type using thresholds from empirical measurements. Since liquid will always submerge the bottom pixel first, the ratio can also serve as an activation for both liquid type and level detection such that we do not start predicting if the bottom pixel is not fully submerged in the liquid and the ratio is too small.
- **Liquid Level Detection:** From our observation, the first derivatives of neighbouring pixel measurements are always at the largest for the pixels closest to the liquid level. Therefore, we rank the gradients of neighbouring pixels, selecting the top two largest gradients  $w_1, w_2$  and identifying their corresponding upper pixel heights  $h_1, h_2$ , and use those gradients as weights to interpolate the liquid level as weighted average  $h = (w_1 h_1 + w_2 h_2) / (w_1 + w_2)$ .

Our 1D liquid sensing prototype has  $1 \times 8$  photodetectors with 15.2 mm between pixels, summing to an effective measurement range of about 110 mm. We collected data using a transparent glass cup with 4 types of drinks (black coffee, sweet tea, orange soda, and milk), 3 indoor lighting conditions (250 lux, 500 lux and 750 lux), and 21 liquid levels from 0 to 100 mm with 5 mm intervals, for a total of  $4 \times 3 \times 21 \times 8 = 2106$  data points. The result of liquid type detection and the root mean squared error (RMSE) of liquid level detection versus actual liquid level is shown in Fig. 7.

Based on the measurement, the ratio for liquid type classification was chosen to be no liquid: [0, 0.1], orange soda: [0.1, 0.39], sweet tea: [0.39, 0.6], black coffee: [0.6, 0.83], and milk: [0.83, 1]. The classification rule was quite robust across all lighting conditions, leading to an overall accuracy of 90.35%. For the liquid level detection, our

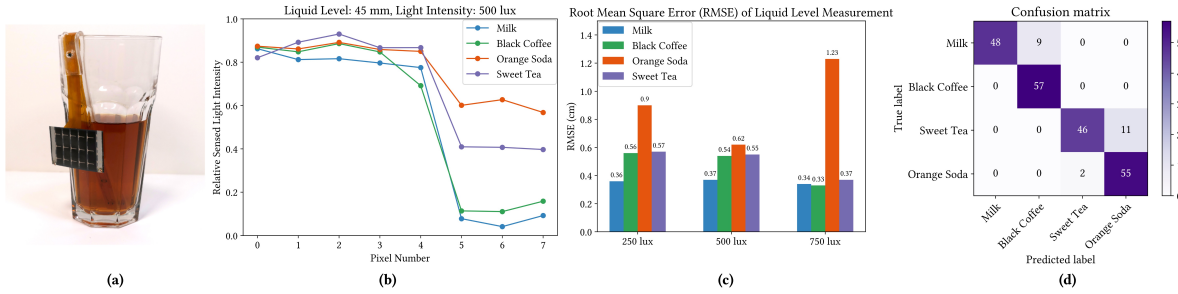


Fig. 7. (a) 1D OptoSense used for liquid sensing. (b) Raw signal in a 500 lux ambient light environment and liquid level at 45 mm for four types of liquid. (c) RMSE of liquid level detection and (d) confusion matrix for liquid type detection averaged over all ambient light conditions.

approach has led to an average RMSE of 5.6 mm across all lighting conditions. Milk was the most accurate, with an average RMSE of 3.6 mm compared to orange soda with an average RMSE of 9.1 mm. The average RMSE of liquid level detection was similar across all lighting conditions. The results indicate that the liquid level detection is more accurate for light-absorbent types and less for the transparent types. We believe the less distinctive liquid-air gradients for the latter contributed to the error of liquid level measurement.

While we only collected data for liquid sensing in a transparent glass container, we observed that it would also work for non-transparent containers such as a ceramic mug. The pixels lower to the bottom of the mug receive less ambient light due to occlusions such that calibration is needed. Users can take measurements in an empty mug once to record background ambient light intensities for future uses. Our liquid sensing is based on visible light absorption by the liquid, which will not work for transparent liquids such as water. However, OptoSense can use narrow-band photodetectors to sense liquids that absorb light outside the visible spectrum (e.g., infrared or ultraviolet for water detection) or to detect the color of the liquid for more granular liquid type detection.

#### 6.4 Walking Activity Detection

With a flexible form factor, the **1D** photodetector array with **wide** FoVs can be wrapped around a user's wrist like a wristband to sense walking activity from an **allocentric** perspective. As the user walks, their arms swing back and forth, creating periodic occlusions between their arms and torso. With photodetectors to sense the oscillating light patterns, we can use the information to detect walking activity and do step counting in a more energy efficient way compared to other technologies such as inertial measurement units (IMUs).

We use the same  $1 \times 8$  photodetector array on polyimide substrate for this step counting application. For our system to work, the user just needs to wrap the wristband on either arm in any orientation. The rationale is that there will be photodetectors facing inward toward the body and away from the body, and our algorithm will automatically detect the orientation from the user's walking activity. For step counting, our approach is also rule-based; it is computationally inexpensive yet robust against changing ambient light. Our algorithms for step counting is as follows:

- **Orientation Calibration:** We calibrate the orientation and identify the pixels facing the body (signal + reference) or facing outward (reference) as the user takes a few steps. We calculate the standard deviation of each pixel from a few seconds of pixel data, and we use the two pixels of highest standard deviation as body-facing and the lowest two as outward-facing.
- **Step Counting:** We calculate the means of body-facing and outward-facing pixels and use the difference between the two as a signal for step counting. From the signal we calculate the first derivatives between

two time frames as an indicator. When the arm swings past body the indicator is at its maximum positive or negative value depending on its motion direction. We identify these peaks with an empirical threshold and use the number of peaks as the steps of the user. The signs of the peaks can be used to identify the left and right steps depending on which arm wears the sensor.

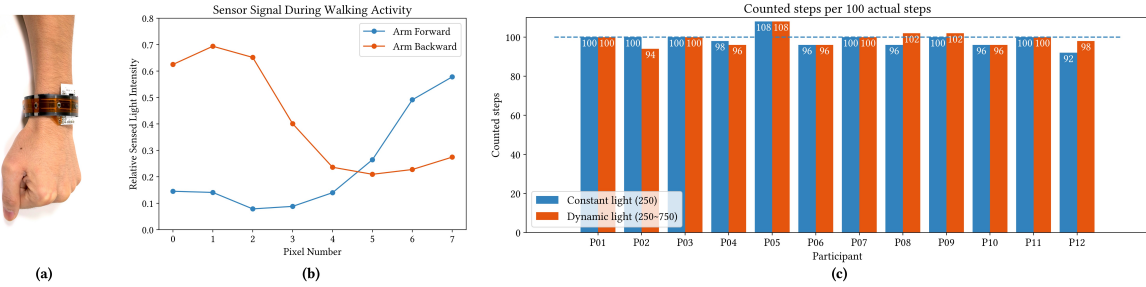


Fig. 8. (a) 1D OptoSense used as step-counting wristband and (b) its raw signal when arm swings to the maximum magnitude in the opposite direction. (c) Step counting results for 12 participants in constant and dynamic ambient lighting.

We conducted the evaluation on 12 participants (10 male, 2 female) in the lab. We asked them to wear the wristband on either of their arms and walk at a normal speed in an approximately 4 m x 6 m loop, counting their steps aloud for every other step. The software uses the first ten seconds of data for orientation calibration and then begins counting steps. We let the user walk 100 steps after the calibration was done and recorded the detected steps. We conducted the walking experiment in two sessions of constant and dynamic ambient lighting environment. In the first session, light was near uniform (~250 lux) on the walking path with regular ceiling illumination; in the second session, we provided additional lights to increase the light intensity at one side of the loop to 750 lux while the other side remained at 250 lux, such that the user would be walking in dynamic ambient light of 250-750 lux. In total we collected 2 conditions  $\times$  100 steps  $\times$  12 participants = 2400 steps. As shown in Fig. 8, an average of 98.8 (SD = 3.86) of the 100 steps were detected under constant light and 99.3 (SD = 3.75) under dynamic light. Overall, the algorithm has shown robust performance in different ambient lighting environments.

The 1D OptoSense can be also used to classify other activities such as arm curls or jumping jacks, or it can be moved to other on-body locations. Ambient light-based step counting would not work well if the wristband is covered by sleeves, or if the user is walking without swinging their arms (e.g., with hands in pockets or holding bags), or if the user's arm swing is too weak. These situations can be avoided by moving the 1D OptoSense onto shoe collars.

## 6.5 Indoor Traffic Sensing

By **narrowing** the sensors' FoVs and extending their range of sensing via an optical mask with 10 mm light tunnels, we developed **1D** OptoSense for indoor traffic sensing (Fig. 13 (b)) from an **egocentric** perspective. The system can be mounted on the wall of a hallway or next to an entry or exit, or on the shelf of a retail store to sense a passing human and their direction of motion for indoor traffic control or surveying purposes. For situations where it is critical in monitoring room occupancy, indoor traffic, or social distances, OptoSense can be deployed close the entry, exit, or on the line-keeping stanchions to monitor traffic flow. The sensors can detect human motion at a distance of one meter using a 1D version of Motion History Images (MHI) and Global Gradient Orientation described by Bradski and Davis [5]. Unlike commonly used off-the-shelf passive infrared (PIR) sensors which can only detect the presence of motion, our system can detect both the speed and direction of motion, and has a flexible form factor that can fit in corners or curved surfaces.

We evaluated the modified 1D  $1 \times 8$  OptoSense with 10 participants (8 male, 2 female) in a hallway of 250 lux illumination. The system was instrumented on the wall at the height of one meter, parallel to the floor and facing the opposite wall. Participants were instructed to walk past the sensor at a one meter distance with their normal walking speed, in both directions, for a total of 20 times. In sum, we collected  $20 \text{ trials} \times 2 \text{ directions} \times 10 \text{ participants} = 400 \text{ samples}$ . The overall accuracy of indoor traffic detection was 91% ( $\text{SD} = 4.25$ ) across all participants, with a false negative rate of 6.8%. Fig. 13 (b) shows the system setup and the confusion matrix of the results. We did not observe false positives when participants stood by before or after walking.

As with the 0D presence detection application, we observed similar effects of the user's body frame and color of clothes on both the detection range and false negative rates. In this application scenario of hallways, the sensors are typically facing another wall within a few meters, such that the contrast between the user's clothes and the wall will have a greater effect on detection. Using narrow-band (e.g., visible, infrared) optical filters or photodetectors to detect subtle differences of light signals can compensate for the effect. Also, the current system cannot distinguish multiple persons in its FoV, which can be compensated by using multiple systems at different locations.

## 7 EXPLICIT INTERACTIONS ON EVERYDAY SURFACES

We now discuss the use of OptoSense to enable touch and hover interactions on everyday surfaces. Specifically, we implement and evaluate 2D sensors for multitouch and hover inputs (Fig. 9). For hover inputs, we also investigate using an optical mask for extending its sensing range. Similar to the previous section, algorithms for 2D OptoSense are designed and run on a low-power platform with rule-based methods.

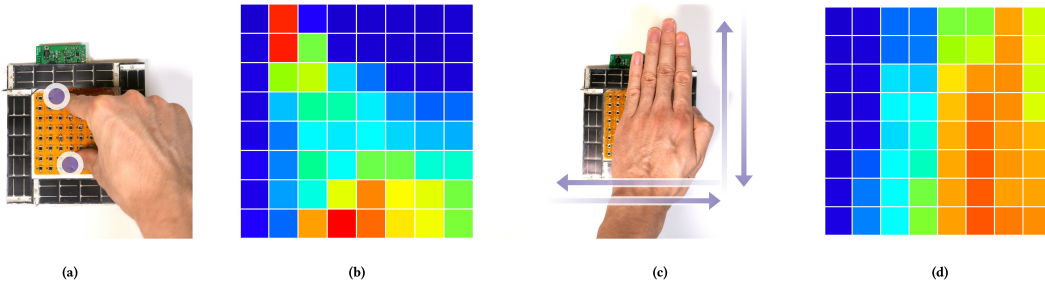


Fig. 9. 2D OptoSense used for interactions: (a) multitouch and (c) hover input. (b)(d) Raw signals of 2D photodetector arrays are rendered with a heatmap.

### 7.1 Multitouch Input

Multitouch input on OptoSense is designed to use continuous tracking of finger touch locations similar to a trackpad, using 2D sensors with **wide** FoVs in an **egocentric** perspective. There are many scenarios where a self-powered interactive surface capable of detecting 2D multitouch input would be desirable, particularly when interactive surfaces are integrated into large everyday surfaces (e.g., walls, windows, furniture, etc.) or mobile objects where tethered power or batteries are not preferable (e.g., cups, garments, frames, etc.). For instance, OptoSense can be used for note taking on walls; collaborative sketching in a meeting room; volume, light or temperature controls on electric appliances; or emergency buttons that can be widely distributed. Compared to capacitive or resistive touch sensing, OptoSense can work with objects not capacitively coupled to ground (e.g., while wearing gloves, using a stylus or even a laser pointer), can be contact-free, and is self-powered. OptoSense can be wirelessly connected using a standard Bluetooth Human Interface Device (HID) profile to BLE-enabled

devices such as smartphones and smart hubs that support interactive applications or relay input events to the cloud.

To extract the touch location, we again apply low-power  $O(n)$  complexity algorithms to the ambient light blocking ratio  $\phi$  of 2D photodetector arrays, where  $n$  is the total number of pixels. Photodetectors periodically measure ambient light intensities and use this value as background should the signal be stable between frames. During an interaction, the instantaneous signal strength of  $\phi$  from one or multiple photodetectors surpasses a threshold, and an input event is detected. The threshold is dynamic and can adjust itself based on the ambient light background. To extract the locations of touch points, we use the Vincent-Soille watershed algorithm [42] for region-based segmentation and extraction of local minima. After segmenting the regions of each touch point, we extract the  $(x, y)$  location of touch points by center of mass and assign an ID for each. Time complexity of this entire procedure is  $O(n)$ . To track the IDs of touch points between two sequential frames, the Minimum Distance First (MDF) method described by Simmons et al. [47] is used with a time complexity at most  $O(m^2)$ , where  $m$  is the number of points being tracked; in our case  $m = 5$ . Depending on the use case, we can adjust the number of tracked touch points from single touch where  $m = 1$ , to potentially multi-user interactions, e.g.,  $m = 20$ .

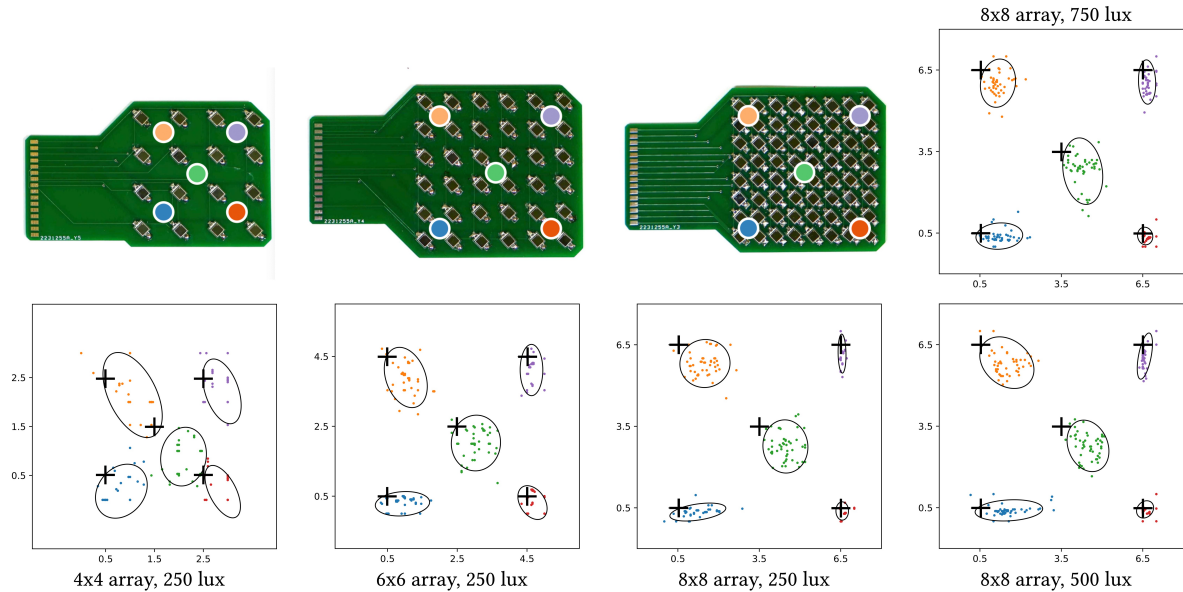


Fig. 10. Five touch locations on the 2D photodetector array with three resolutions. The detected touch locations are rendered with 95% eclipses on relative scales with the desired locations marked with crosses.

To evaluate the performance of touch input, we conducted an evaluation on 12 participants (10 male, 2 female; 2 left- and 10 right-handed; length of index finger 8.2~11.5 cm (Mean = 9.4, SD = 0.86)). Each participant was asked to touch five locations on the photodetector array {top left, top right, center, bottom left, bottom right} with the index finger of the dominant hand, one location at a time. The set of locations was selected to cover the entire range of possible touch locations in 2D. We explicitly picked locations centered between four neighboring pixels (Fig. 10) to fully test how pixel resolution affects touch sensing. Each touch location was repeated four times, and the entire set was randomized.

We investigated two factors which can potentially affect our sensing performance – resolution and ambient light intensity. While keeping the surface area the same size of 50 mm × 50 mm, we varied the resolution of the

photodetector array to be  $\{4 \times 4, 6 \times 6, 8 \times 8\}$  which corresponds to an inter-pixel distance of  $\{6, 9, 12\}$  mm while fixing the ambient light intensity to 250 lux. Then we varied the ambient light intensity to  $\{250, 500, 750\}$  lux while using the  $8 \times 8$  array. The order of test conditions within the same category was arranged with a 3x3 Latin square. In total, 1200 touch trials were collected (5 locations  $\times$  4 repetitions  $\times$  5 conditions  $\times$  12 participants).

The detected touch locations of all participants are rendered in Fig. 10, with Fig. 11 showing the analysis. On average, we achieved a false negative rate (i.e., percentage of touches missed) of 7.36%. For touch trials that were detected, the overall mean distance error was 5.57 mm (SD = 2.49). During the user study, participants were also asked to hover their finger 3 cm and 1 cm above the 5 locations of sensors for all conditions, and misclassified touches were recorded for false positive investigation. At 3 cm above the photodetector array, the false positive rate was zero, and at 1 cm the overall false positive rate was 19.5%. We did not observe any false positives from participants standing and walking around the sensor (i.e., with no finger or hand hovering above).

As we expected, the pixel resolution has a great impact on the touch tracking accuracy and false negative rate. However, ambient light intensity has a minimal effect on both. Interestingly, we observed that the detected locations deviate to the bottom and right of the desired locations, collocated with the actual pixels blocked from light by the index fingers as 10 out of 12 participants were right-handed. With a finger above at 1 cm, the top left location showed the highest false positive rate of 35% compared to the lowest bottom right of 5%, as more pixels were affected by the shadow of a user's finger and hand. We also noted higher false positive rates at an ambient light intensity of 500 lux (22.7%) and 700 lux (16.8%) compared to 250 lux (5.6%) due to the fact that additional light was provided primarily by direct light from above rather than diffuse light from other directions, which contributed to the high standard deviation in Fig. 11 (d).

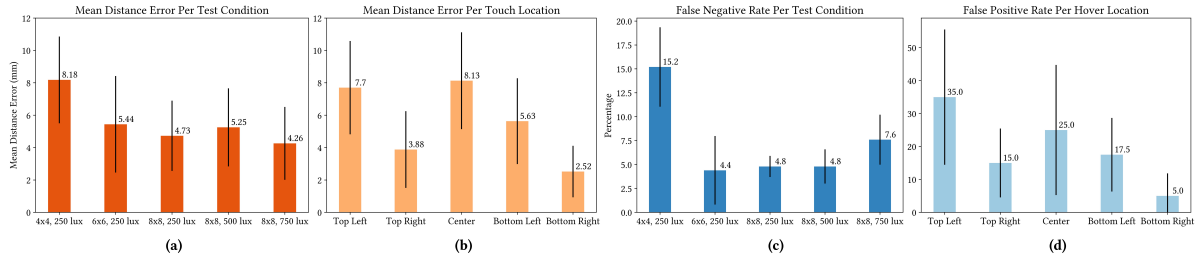


Fig. 11. Result of the 5-point touch study. (a) Mean distance error of detected touch location vs actual location, averaged per test condition and (b) per touch location. (c) Average false positives of hovering finger 1 cm above the touch locations. (d) False negatives averaged per test condition.

The results show that ambient light-based touch detection works best when light comes uniformly from all directions in a mainly diffuse light field and less accurately with a small number of strong direct light sources. Another challenge is the blocking of light from a user's fingers and hands which results in deviations of touch location detection. This issue can be mitigated by having additional knowledge about the object, in our case the size, finger shape, and models of hand-finger association, to implement rejections of palm and false touches for improving touch tracking performance.

## 7.2 Hover Input

Hover input on OptoSense is designed for discrete gestures 1 cm above the surface, using **2D** sensors with **wide** FoVs in an **egocentric** perspective. Having surfaces capable of detecting hovering input enables contactless microinteractions for situations where physical contact is not desirable. For instance, OptoSense can be used for media controls in the kitchen, where the user with dirty hands can gesture to play or pause a cooking tutorial;

interactive displays for public spaces where contact should be avoided for hygiene reasons; or rapid interactions that demand little visual attention, such as switching radio stations while driving.

To investigate hover sensing with OptoSense, we select four exemplar swiping gestures {swipe up, swipe down, swipe left, swipe right} which users can use to interact with smart devices without touch. We use Motion History Images (MHI) and Global Gradient Orientation [5] to extract the direction of swipe gestures. Similar to touch input, we use dynamic thresholding to detect the input event, calculate MHI and its gradient orientation for each frame, and use the average of gradient orientation from all frames to determine the swiping direction. The entire input detection framework has a time complexity of  $O(n)$ .

We conducted the evaluation on the same 12 participants with the same variation of pixel resolution  $\{4 \times 4, 6 \times 6, 8 \times 8\}$  and ambient light  $\{250, 500, 750\}$  lux conditions as the previous touch evaluation. Each participant was asked to perform the 4 swipe gestures  $\times$  5 repetitions = 20 trials in random order per condition, which resulted in a total number of 1200 swipe trials. We also recorded the detection result when participants stood by without performing gestures to investigate false positives.

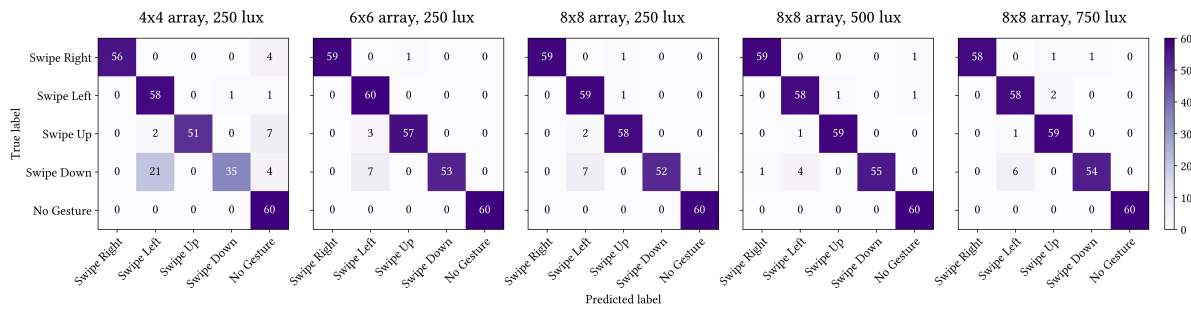


Fig. 12. Confusion matrices for four directional swipes across three pixel resolutions and three ambient light intensities.

Overall, we achieved a 93% accuracy ( $SD = 3.62$ ) across all participants, a zero false positive rate, and a false negative rate of 1.6%. Under 250 lux ambient light, the  $4 \times 4$  array showed the lowest accuracy of 82.2% compared to  $6 \times 6$  of 95.1% and  $8 \times 8$  of 94.7%, and the highest false negative rate of 6.3%, as shown in Fig. 12. We believe that the  $4 \times 4$  resolution is simply too low to capture the motion direction robustly. We also found that the changing ambient light level had minimal effect on the recognition accuracy and false negative rate. While most participants found swiping gestures intuitive and easy to perform, one common feedback was that swipe down was not as effortless as the others as it was both more time-consuming (requires the user to move hand around the sensor to the top position and then perform the swipe down gesture) and also more difficult to keep the path straight. This difficulty was also reflected from the confusion matrices as swipe down was frequently confused with swipe left due to the fact that the majority of the participants were right-handed – they unconsciously shifted their hands to bottom left during the swipe down gesture.

Though the results show promise, we caution that more tests should be done with a wider variety of real-world scenarios. The set of gesture input is also limited to four directions as examples. With higher resolution and potentially the use of machine learning, we envision OptoSense supporting more subtle gestures involving palm, fist, and fingers in the future.

### 7.3 Hover Input with Extended Range

To maintain a high signal-to-noise ratio, the range of hover gesture input demonstrated previously is effective only within around 50 mm above the sensor. Here, we show how in-air gesture input at greater distances can be

achieved using sensors with **narrow** FoVs. Fig. 13 (c) shows an optical mask with  $8 \times 8$  tunnels of 10 mm length attached to 2D OptoSense, increasing the range of input to 200+ mm above the surface. The rest of the system, including the gesture set and the sensing techniques are kept the same as those described in 2D Hover Input.

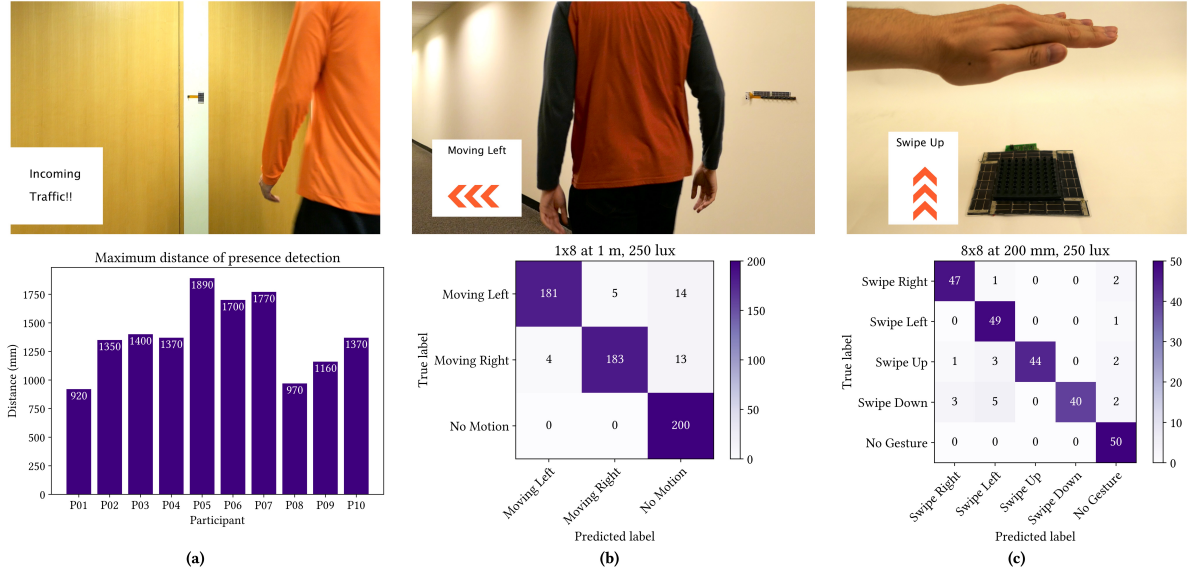


Fig. 13. Extended range applications of OptoSense using optical masks of 10 mm light tunnels: (a) 0D application – presence detection to send alert to the other side of the door. (b) 1D application – indoor traffic detection. (c) 2D application – in-air swiping gesture input at a distance of 20 mm.

We evaluated the modified 2D  $8 \times 8$  OptoSense with 10 participants (8 Male, 2 Female) under 250 lux illumination. Similar to the previous evaluation of swiping gestures, participants were instructed to perform the same set of gestures {swipe up, swipe down, swipe left, swipe right}  $\times$  5 repetitions = 20 trials in random order, which resulted in 200 trials collected in total. The difference was that we asked the participants to perform the swiping gestures in air at 200 mm above the sensing surface.

We achieved an overall 90% accuracy ( $SD = 1.25$ ) across all participants and a false negative rate of 3.5%. This result was comparable to the 94.7% accuracy of the near-surface hover input with the same apparatus but without the optical mask. No false positives were observed when participants stood by without performing gestures. Of the four gestures, swipe up (88%) and swipe down (80%) showed lower accuracy compared to swipe left (98%) and swipe right (94%) since it is more difficult to align with the sensors in this (anteroposterior) axis at a height of 200 mm. Although OptoSense can still detect gestures at a height greater than 200 mm, aiming and alignment with the sensors will become increasingly difficult for the user, which in turn decreases detection accuracy.

## 8 ORGANIC SEMICONDUCTOR DEVICES FOR AMBIENT LIGHT SENSING SURFACES

In the previous sections we demonstrated the feasibility of self-powered ambient light sensing surfaces using off-the-shelf silicon-based photodetectors. For the goal of ubiquitous sensing surfaces, the form factor and the cost for silicon photodetectors are the current main challenges of OptoSense. To address such challenges, we start to investigate the implementation of a fully-flexible 2D photodetector array developed with organic semiconductor (OSC) devices fabricated with an additive manufacturing process.

## 8.1 Emerging Optoelectronics

Emerging optoelectronic devices based on organics, perovskites, 2D and hybrid semiconductors offer exciting possibilities for OptoSense because they can be fabricated at a low cost on flexible substrates. In particular, organic semiconductor (OSC)-based optoelectronic devices offer a promising material platform because they can be processed over large areas at low temperatures using cost-effective high-throughput manufacturing technologies, such as printing and roll-to-roll coating. OSC devices can be fabricated on plastics [48], paper [25, 53, 58] or transfers laminated onto other substrates [19, 69], including stretchable ones [37, 61]. Furthermore, OSC devices can be engineered to be transparent or semitransparent [20, 31, 54, 68, 69], which may enable seamless integration with everyday objects.

## 8.2 2D OSC Photodetector Array: Preliminary Work

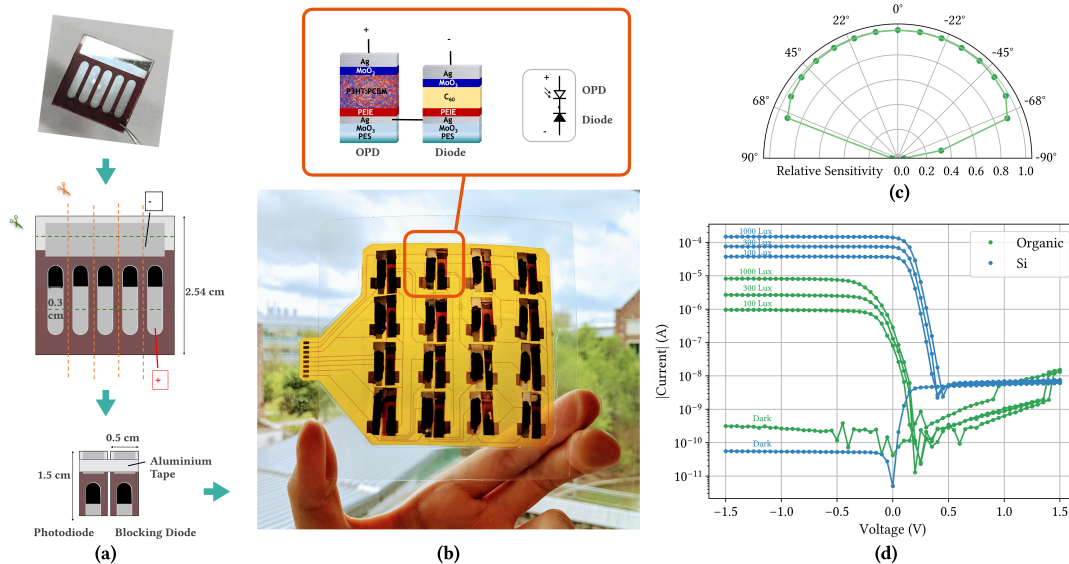


Fig. 14. Sensing surface developed with organic optical sensors. (a) Fabrication process of an organic sensor pixel. (b) A  $4 \times 4$  optical sensor array developed on a polyimide substrate, with each individual pixel using an organic photodiode (OPD) and an organic blocking diode. (c) Angular directivity of the organic optical sensor. (d) Irradiance-dependent steady-state current density vs. voltage (I-V) characteristics of a single pixel comparing organic and silicon devices.

We developed a  $4 \times 4$  optical sensor array with OSC devices fabricated separately and then mounted on a polyimide FPC with conductive adhesive transfer tape (3M 9703), shown in Fig. 14. Each individual pixel consists of an organic photodiode (OPD) and an organic blocking diode connected by their cathodes using aluminum tape. As an electron-collecting electrode, we use a Ag layer coated with polyethylenimine (PEIE). A blend of highly regioregular poly(3-hexylthiophene-2,5Diyl) (P3HT) mixed with [6,6]-phenyl-C<sub>61</sub>-butyric acid methylester (PCBM) is used as the photoactive layer for the OPD, and fullerene (C<sub>60</sub>) for the blocking diode. MoO<sub>3</sub> followed by a Ag layer is used for the hole-collecting electrode/interlayer. Both OPDs and blocking diodes were fabricated using spin coating and thermal evaporation techniques on polyestersulfone (PES) substrates. The entire circuit of the  $4 \times 4$  sensor array was heat laminated with a transparent thermal lamination pouch.

We evaluated the sensor performance by measuring angular directivity and irradiance-dependent steady-state current density vs. voltage (I-V) characteristics of a single pixel. The angular directivity of the organic pixel was measured by varying the incidence angle of a laser beam cast upon the OPD. I-V characteristics were measured by applying an electrical bias to a sensor using the voltage source output of an electrometer (Keithley 2400), averaged over a set period of time. The illumination over the sensor was provided by an incandescent bulb with variable power. We measured 11 sets of illumination levels (0 to 1k lux over the sensor with 100 lux steps)  $\times$  61 sets of voltage bias (-1.5 to 1.5 V with 0.05 V steps) for both organic and silicon (BPW34 + BAS40-02V-V-G) pixels, as shown in Fig. 14 (d).

The organic and silicon pixels displayed comparable optoelectronic properties: low dark current (sub-nA) and high photocurrent ( $\mu$ A) under reverse bias, linear response to irradiance in photoconductive mode, and low leakage current (nA) under forward bias. The FoV of the OPDs was 150° (Fig. 14 (c)). The higher photocurrent of the silicon sensor pixel was due to a higher spectral response of silicon photodiodes in the infrared (IR) range (up to 1100 nm) while OPDs with the proposed photoactive layers absorb light at visible wavelengths up to around 650 nm; our light source (an incandescent bulb) emits heavily in the IR range. Another difference is the switch-on voltage of the blocking diode, which was higher for organic diodes compared to silicon Schottky diodes. This difference makes the I-V curve of an organic pixel “shift left” horizontally compared to silicon. With optimization of the organic diode structure and materials, we can expect to reduce its switch-on voltage.

While individual OSC-based pixels may function as well as a silicon-based ones, we found that the manual cut-and-paste assembly process introduced high inter-pixel variability and crosstalk to the circuit. This observation demonstrates the need for a monolithic fabrication process of the entire array to ensure uniform performance across all pixels for 2D imaging. Such a process is also desired for fully-automated large scale manufacturing. Furthermore, it is also desirable to use such manufacturing to produce OPV devices for energy harvesting in an OSC-based OptoSense system.

## 9 DISCUSSION

We have demonstrated a self-powered ambient light sensing platform with a variety of form factors and discussed the requirement of scaling up the system in terms of power. Here we discuss other critical factors including ambient light, latency, and cost.

*Ambient Light:* OptoSense is limited in its ability to sense objects that barely absorb light, such as water or other transparent items. It also will not work without ambient light, such as in dark environments. We considered ambient light illumination conditions that reflect real world scenarios in our evaluations. Specifically, we studied how ambient light intensities affect the sensing of “quick” interactions such as door opening and hover input using three ambient light levels (250, 500, and 750 lux) and varied the ambient light intensity (oscillating between 250 and 750 lux) during the study for the “prolonged” walking activity. The results showed our methods were robust against ambient light variations under these conditions. Darker lighting conditions might occur in practice, though human activities are often inseparable from some ambient light. Fortunately, Si photodetectors are sensitive even under 100 lux with a large load resistance (e.g., 1 M $\Omega$ ). For handling both dark conditions as well as more regular ambient lighting, automatic adjustment of load resistance could be implemented with digital potentiometers (DigiPOT).

*Latency:* Another important metric of our system is latency. The time required for wireless communication is not affected by the number of pixels since the detection result being communicated is of fixed length; however, signal acquisition and local computation is affected by the number of pixels. For instance, each ADC sampling takes 10 $\mu$ s, resulting in our 8  $\times$  8 system requiring at least 0.64 ms for sampling all pixels. We found this refresh rate fast enough for interactive systems, and even systems with larger scales – a system with 100  $\times$  100 pixels

should take around 0.1s to complete one frame, though “rolling shutter” effects might be caused by these minute delays. In that case, a circuit design with a global shutter might be desired.

**Cost:** All components of OptoSense are low-cost: microprocessor \$2.87, photovoltaic \$0.06/cm<sup>2</sup>, and photodiode \$0.31. Considering that the number of photodiodes is proportional to the sensing area, one major cost in large-scale ambient light sensing surfaces is the silicon photodiodes. Although no OPD is available in the market, commodity OPVs can be found for around \$0.01/cm<sup>2</sup> [17], and some experts estimate the cost can be as low as \$0.001/cm<sup>2</sup> [3]. We estimate the cost of large-scale systems can be reduced by at least 90% with the use of OSC devices.

## 10 CONCLUSION

In this work we presented the OptoSense system as a self-powered ambient light sensing surface for activity sensing and interactions. We provided a design framework of self-powered ambient light sensing surfaces and developed a variety of applications based on different design choices of activity type, sensing dimensions, sensing range, and sensing perspective. We demonstrated OptoSense as a versatile, robust, accurate, and privacy-compliant sensing technology. To address the limitations of silicon-based devices, we investigated the use of OSC devices, showing a promising direction for ambient light sensing in future work. OptoSense has shown advances over prior work by unlocking unique sensing modalities. Taken together, we believe our sensing framework, system implementation, and findings through evaluations will make ubiquitous sensing and a wide range of applications more practical in the future.

## ACKNOWLEDGMENTS

We thank Tavenner Hall for her advice and help in writing the paper, Yiming Lyu for creating the sketch of application scenarios in Fig. 1, our anonymous reviewers, and user study participants for their contributions.

## REFERENCES

- [1] Michelle Annett, Tovi Grossman, Daniel Wigdor, and George Fitzmaurice. 2011. Medusa: a proximity-aware multi-touch tabletop. ACM, 337–346.
- [2] Nivedita Arora, Steven L. Zhang, Fereshteh Shahmiri, Diego Osorio, Yi-Cheng Wang, Mohit Gupta, Zhengjun Wang, Thad Starner, Zhong Lin Wang, and Gregory D. Abowd. 2018. SATURN: A thin and flexible self-powered microphone leveraging triboelectric nanogenerator. *Proceedings of the ACM on Interactive, Mobile, Wearable and Ubiquitous Technologies* 2, 2 (2018), 60.
- [3] Zach M. Bailey and Michael D. McGehee. 2012. Modeling low cost hybrid tandem photovoltaics with the potential for efficiencies exceeding 20%. *Energy & Environmental Science* 5, 11 (2012), 9173. <https://doi.org/10.1039/c2ee23073a>
- [4] Fred W. Billmeyer. 1981. IES Lighting Handbooks, 1981 Reference Volume and 1981 Applications Volume, John E. Kaufman, Ed. Illuminating Engineering Society of North America, New York, 1981, 500 pp. each. Price: \$50.00 each, \$90.00 set. *Color Research & Application* 6, 4 (1981), 253–253. <https://doi.org/10.1002/col.5080060417>
- [5] Gary R. Bradski and James W. Davis. 2002. Motion segmentation and pose recognition with motion history gradients. *Machine Vision and Applications* 13, 3 (July 2002), 174–184. <https://doi.org/10.1007/s001380100064>
- [6] Francesca Brunetti, Alessandra Operamolla, Sergio Castro-Hermosa, Giulia Lucarelli, Valerio Manca, Gianluca M. Farinola, and Thomas M. Brown. 2019. Printed Solar Cells and Energy Storage Devices on Paper Substrates. *Advanced Functional Materials* 29, 21 (May 2019), 1806798. <https://doi.org/10.1002/adfm.201806798>
- [7] Alex Butler, Shahram Izadi, and Steve Hodges. 2008. SideSight: multi-touch interaction around small devices. ACM, 201–204.
- [8] Tim Campbell, Eric Larson, Gabe Cohn, Jon Froehlich, Ramses Alcaide, and Shwetak N. Patel. 2010. WATTR: A Method for Self-powered Wireless Sensing of Water Activity in the Home. In *Proceedings of the 12th ACM International Conference on Ubiquitous Computing (UbiComp '10)*. ACM, New York, NY, USA, 169–172. <https://doi.org/10.1145/1864349.1864378>
- [9] Chia-Yuan Chen, Zih-Hong Jian, Shih-Han Huang, Kun-Mu Lee, Ming-Hsuan Kao, Chang-Hong Shen, Jia-Min Sheh, Chin-Li Wang, Chiung-Wen Chang, Bo-Zhi Lin, Ching-Yao Lin, Ting-Kuang Chang, Yun Chi, Cheng-Yu Chi, Wei-Ting Wang, Yian Tai, Ming-De Lu, Yung-Liang Tung, Po-Ting Chou, Wen-Ti Wu, Tahsin J. Chow, Peter Chen, Xiang-Hao Luo, Yuh-Lang Lee, Chih-Chung Wu, Chih-Ming Chen, Chen-Yu Yeh, Miao-Syuan Fan, Jia-De Peng, Kuo-Chuan Ho, Yu-Nan Liu, Hsiao-Yi Lee, Chien-Yu Chen, Hao-Wu Lin, Chia-Te Yen, Yu-Ching Huang, Cheng-Si Tsao, Yu-Chien Ting, Tzu-Chien Wei, and Chun-Guey Wu. 2017. Performance Characterization of Dye-Sensitized Photovoltaics under Indoor Lighting. *The Journal of Physical Chemistry Letters* 8, 8 (April 2017), 1824–1830. <https://doi.org/10.1021/acs.jpcllett.7b00515>

- [10] Ben S. Cook, T. Le, S. Palacios, A. Traille, and M. M. Tentzeris. 2013. Only skin deep: Inkjet-printed zero-power sensors for large-scale RFID-integrated smart skins. *IEEE Microwave Magazine* 14, 3 (2013), 103–114.
- [11] Daniel Groeger and Jürgen Steinle. 2018. ObjectSkin: augmenting everyday objects with hydroprinted touch sensors and displays. *Proceedings of the ACM on Interactive, Mobile, Wearable and Ubiquitous Technologies* 1, 4 (2018), 134.
- [12] Jiseong Gu, Seongkook Heo, Jaehyun Han, Sunjun Kim, and Geehyuk Lee. 2013. LongPad: a touchpad using the entire area below the keyboard of a laptop computer. ACM, 1421–1430.
- [13] Steve Hodges, Shahram Izadi, Alex Butler, Alban Rustemi, and Bill Buxton. 2007. ThinSight: versatile multi-touch sensing for thin form-factor displays. ACM, 259–268.
- [14] Ramon Hofer, Daniel Naeff, and Andreas Kunz. 2009. FLATIR: FTIR multi-touch detection on a discrete distributed sensor array. ACM, 317–322.
- [15] Marc Hubert, Marie Dumont, and Jean Paquet. 1998. Seasonal and Diurnal Patterns of Human Illumination Under Natural Conditions. *Chronobiology International* 15, 1 (Jan. 1998), 59–70. <https://doi.org/10.3109/07420529808998670>
- [16] Guy B Immega and Glenn H Chapman. 1998. *Vision system and proximity detector*. Google Patents.
- [17] infinityPV. 2020. *infinityPV - Panels*. <https://infinitypv.com/products/opv/panels>
- [18] Hiroshi Ishii and Brygg Ullmer. 1997. Tangible bits: towards seamless interfaces between people, bits and atoms. ACM, 234–241.
- [19] Xiaojia Jia, Canek Fuentes-Hernandez, Cheng-Yin Wang, Youngrak Park, and Bernard Kippelen. 2018. Stable organic thin-film transistors. *Science advances* 4, 1 (2018), eaao1705.
- [20] Youyu Jiang, Bangwu Luo, Fangyuan Jiang, Fuben Jiang, Canek Fuentes-Hernandez, Tiefeng Liu, Lin Mao, Sixing Xiong, Zaifang Li, and Tao Wang. 2016. Efficient colorful perovskite solar cells using a top polymer electrode simultaneously as spectrally selective antireflection coating. *Nano letters* 16, 12 (2016), 7829–7835.
- [21] Hsin-Liu Cindy Kao, Christian Holz, Asta Roseway, Andres Calvo, and Chris Schmandt. 2016. DuoSkin: rapidly prototyping on-skin user interfaces using skin-friendly materials. ACM, 16–23.
- [22] Yoshihiro Kawahara, Steve Hodges, Benjamin S. Cook, Cheng Zhang, and Gregory D. Abowd. 2013. Instant inkjet circuits: lab-based inkjet printing to support rapid prototyping of UbiComp devices. ACM, 363–372.
- [23] Roberta L. Klatzky. 1998. Allocentric and Egocentric Spatial Representations: Definitions, Distinctions, and Interconnections. In *Spatial Cognition: An Interdisciplinary Approach to Representing and Processing Spatial Knowledge*, Christian Freksa, Christopher Habel, and Karl F. Wender (Eds.). Springer Berlin Heidelberg, Berlin, Heidelberg, 1–17. [https://doi.org/10.1007/3-540-69342-4\\_1](https://doi.org/10.1007/3-540-69342-4_1)
- [24] Sven Kratz and Michael Rohs. 2009. HoverFlow: expanding the design space of around-device interaction. ACM, 4.
- [25] Lucia Leonat, Matthew Schuette White, Eric Daniel Głowacki, Markus Clark Scharber, Tino Zillger, Julia Rühling, Arved Hübler, and Niyazi Serdar Sariciftci. 2014. 4% efficient polymer solar cells on paper substrates. *The Journal of Physical Chemistry C* 118, 30 (2014), 16813–16817.
- [26] Hanchuan Li, Eric Brockmeyer, Elizabeth J. Carter, Josh Fromm, Scott E. Hudson, Shwetak N. Patel, and Alanson Sample. 2016. Paperid: A technique for drawing functional battery-free wireless interfaces on paper. ACM, 5885–5896.
- [27] Tianxing Li, Chuankai An, Zhao Tian, Andrew T. Campbell, and Xia Zhou. 2015. Human sensing using visible light communication. ACM, 331–344.
- [28] Tianxing Li, Qiang Liu, and Xia Zhou. 2016. Practical human sensing in the light. ACM, 71–84.
- [29] Yichen Li, Tianxing Li, Ruchir A. Patel, Xing-Dong Yang, and Xia Zhou. 2018. Self-powered gesture recognition with ambient light. ACM, 595–608.
- [30] Vincent Liu, Aaron Parks, Vamsi Talla, Shyamnath Gollakota, David Wetherall, and Joshua R. Smith. 2013. Ambient backscatter: wireless communication out of thin air, Vol. 43. ACM, 39–50.
- [31] Dong Ma, Guohao Lan, Mahbub Hassan, Wen Hu, Mushfika B. Upama, Ashraf Uddin, and Moustafa Youssef. 2019. SolarGest: Ubiquitous and Battery-free Gesture Recognition using Solar Cells. In *The 25th Annual International Conference on Mobile Computing and Networking (MobiCom '19)*. Association for Computing Machinery, Los Cabos, Mexico, 1–15. <https://doi.org/10.1145/3300061.3300129>
- [32] Ian Mathews, Sai Nithin Kantareddy, Tonio Buonassisi, and Ian Marius Peters. 2019. Technology and Market Perspective for Indoor Photovoltaic Cells. *Joule* 3, 6 (June 2019), 1415–1426. <https://doi.org/10.1016/j.joule.2019.03.026>
- [33] Jon Moeller and Andriud Kerne. 2012. ZeroTouch: an optical multi-touch and free-air interaction architecture. ACM, 2165–2174.
- [34] K. W. Mui and L. T. Wong. 2006. Acceptable Illumination Levels for Office Occupants. *Architectural Science Review* 49, 2 (June 2006), 116–119. <https://doi.org/10.3763/asre.2006.4915>
- [35] Saman Naderiparizi, Aaron N. Parks, Zerina Kapetanovic, Benjamin Ransford, and Joshua R. Smith. 2015. WISPCam: A battery-free RFID camera. IEEE, 166–173.
- [36] Shree K. Nayar, Daniel C. Sims, and Mikhail Fridberg. 2015. Towards self-powered cameras. IEEE, 1–10.
- [37] Jin Young Oh, Simon Rondeau-Gagné, Yu-Cheng Chiu, Alex Chortos, Franziska Lissel, Ging-Ji Nathan Wang, Bob C. Schroeder, Tadanori Kurosawa, Jeffrey Lopez, and Toru Katsumata. 2016. Intrinsically stretchable and healable semiconducting polymer for organic transistors. *Nature* 539, 7629 (2016), 411.

- [38] Alex Olwal, Jon Moeller, Greg Priest-Dorman, Thad Starner, and Ben Carroll. 2018. I/O Braid: Scalable Touch-Sensitive Lighted Cords Using Spiraling, Repeating Sensing Textiles and Fiber Optics. ACM, 485–497.
- [39] Ivan Poupyrev, Nan-Wei Gong, Shihoh Fukuhara, Mustafa Emre Karagozler, Carsten Schwesig, and Karen E. Robinson. 2016. Project Jacquard: interactive digital textiles at scale. ACM, 4216–4227.
- [40] Vaishnavi Ranganathan, Sidhant Gupta, Jonathan Lester, Joshua R. Smith, and Desney Tan. 2018. Rf bandaid: A fully-analog and passive wireless interface for wearable sensors. *Proceedings of the ACM on Interactive, Mobile, Wearable and Ubiquitous Technologies* 2, 2 (2018), 79.
- [41] Christian Rendl, Patrick Greindl, Michael Haller, Martin Zirkl, Barbara Stadlober, and Paul Hartmann. 2012. PyzoFlex: printed piezoelectric pressure sensing foil. ACM, 509–518.
- [42] Jos BTM Roerdink and Arnold Meijster. 2000. The watershed transform: Definitions, algorithms and parallelization strategies. *Fundamenta informaticae* 41, 1, 2 (2000), 187–228.
- [43] Alanson P. Sample, Daniel J. Yeager, Pauline S. Powledge, Alexander V. Mamishev, and Joshua R. Smith. 2008. Design of an RFID-based battery-free programmable sensing platform. *IEEE Transactions on Instrumentation and Measurement* 57, 11 (2008), 2608–2615.
- [44] Albrecht Schmidt. 2000. Implicit human computer interaction through context. *Personal Technologies* 4, 2 (June 2000), 191–199. <https://doi.org/10.1007/BF01324126>
- [45] Fereshteh Shahmiri, Chaoyu Chen, Anandghan Waghmare, Dingtian Zhang, Shivan Mittal, Steven L. Zhang, Yi-Cheng Wang, Zhong Lin Wang, Thad E. Starner, and Gregory D. Abowd. 2019. Serpentine: A Self-Powered Reversibly Deformable Cord Sensor for Human Input. In *Proceedings of the 2019 CHI Conference on Human Factors in Computing Systems (CHI '19)*. Association for Computing Machinery, Glasgow, Scotland UK, 1–14. <https://doi.org/10.1145/3290605.3300775>
- [46] Nathan S. Shenck and Joseph A. Paradiso. 2001. Energy scavenging with shoe-mounted piezoelectrics. *IEEE micro* 3 (2001), 30–42.
- [47] Martin Simmons, Daniel Pickett, Martin Simmons, and Daniel Pickett. 2014. Multi-touch tracking. <https://patents.google.com/patent/US8866790B2/en>
- [48] Takao Someya, Siegfried Bauer, and Martin Kaltenbrunner. 2017. Imperceptible organic electronics. *MRS Bulletin* 42, 2 (2017), 124–130.
- [49] T. Starner, D. Kirsch, and S. Assefa. 1997. The locust swarm: an environmentally-powered, networkless location and messaging system. In *Digest of Papers. First International Symposium on Wearable Computers*. IEEE Comput. Soc, Cambridge, MA, USA, 169–170. <https://doi.org/10.1109/ISWC.1997.629938>
- [50] Vamsi Talla, Mehrdad Hessar, Bryce Kellogg, Ali Najafi, Joshua R. Smith, and Shyamnath Gollakota. 2017. Lora backscatter: Enabling the vision of ubiquitous connectivity. *Proceedings of the ACM on Interactive, Mobile, Wearable and Ubiquitous Technologies* 1, 3 (2017), 105.
- [51] Vamsi Talla, Bryce Kellogg, Shyamnath Gollakota, and Joshua R. Smith. 2017. Battery-Free Cellphone. *Proc. ACM Interact. Mob. Wearable Ubiquitous Technol.* 1, 2 (June 2017), 25:1–25:20. <https://doi.org/10.1145/3090090>
- [52] Stuart Taylor, Cem Keskin, Otmar Hilliges, Shahram Izadi, and John Helmes. 2014. Type-hover-swipe in 96 bytes: a motion sensing mechanical keyboard. ACM, 1695–1704.
- [53] Daniel Tobjörk and Ronald Österbacka. 2011. Paper electronics. *Advanced Materials* 23, 17 (2011), 1935–1961.
- [54] Jinhui Tong, Sixing Xiong, Yifeng Zhou, Lin Mao, Xue Min, Zaifang Li, Fangyuan Jiang, Wei Meng, Fei Qin, and Tiefeng Liu. 2016. Flexible all-solution-processed all-plastic multijunction solar cells for powering electronic devices. *Materials Horizons* 3, 5 (2016), 452–459.
- [55] Hoang Truong, Shuo Zhang, Ufuk Muncuk, Phuc Nguyen, Nam Bui, Anh Nguyen, Qin Lv, Kaushik Chowdhury, Thang Dinh, and Tam Vu. 2018. CapBand: Battery-free Successive Capacitance Sensing Wristband for Hand Gesture Recognition. ACM, 54–67.
- [56] Ambuj Varshney, Andreas Soleiman, Luca Mottola, and Thiembo Voigt. 2017. Battery-free visible light sensing. ACM, 3–8.
- [57] Raghav H. Venkatnarayan and Muhammad Shahzad. 2018. Gesture recognition using ambient light. *Proceedings of the ACM on Interactive, Mobile, Wearable and Ubiquitous Technologies* 2, 1 (2018), 40.
- [58] Cheng-Yin Wang, Canek Fuentes-Hernandez, Wen-Fang Chou, and Bernard Kippelen. 2017. Top-gate organic field-effect transistors fabricated on paper with high operational stability. *Organic Electronics* 41 (2017), 340–344.
- [59] Mark Weiser. 1991. The computer for the 21st century. *Scientific american* 265, 3 (1991), 94–104. <http://www.nature.com/scientificamerican/journal/v265/n3/full/scientificamerican0991-94.html>
- [60] Raphael Wimmer. 2010. FlyEye: grasp-sensitive surfaces using optical fiber. ACM, 245–248.
- [61] Jie Xu, Sihong Wang, Jing-Ji Nathan Wang, Chenxin Zhu, Shaochuan Luo, Lihua Jin, Xiaodan Gu, Shucheng Chen, Vivian R. Feig, and John WF To. 2017. Highly stretchable polymer semiconductor films through the nanoconfinement effect. *Science* 355, 6320 (2017), 59–64.
- [62] Zhice Yang, Zeyu Wang, Jiansong Zhang, Chenyu Huang, and Qian Zhang. 2015. Wearables Can Afford: Light-weight Indoor Positioning with Visible Light. In *Proceedings of the 13th Annual International Conference on Mobile Systems, Applications, and Services - MobiSys '15*. ACM Press, Florence, Italy, 317–330. <https://doi.org/10.1145/2742647.2742648>
- [63] Yang Zhang and Chris Harrison. 2018. Pulp nonfiction: Low-cost touch tracking for paper. ACM, 117.
- [64] Yang Zhang, Yasha Iravantchi, Haojian Jin, Swarun Kumar, and Chris Harrison. 2019. Sozu: Self-Powered Radio Tags for Building-Scale Activity Sensing. In *Proceedings of the 32Nd Annual ACM Symposium on User Interface Software and Technology (UIST '19)*. ACM, New York, NY, USA, 973–985. <https://doi.org/10.1145/3332165.3347952>

- [65] Yang Zhang, Gierad Laput, and Chris Harrison. 2017. Electrick: Low-cost touch sensing using electric field tomography. ACM, 1–14.
- [66] Yang Zhang, Chouchang Jack Yang, Scott E. Hudson, Chris Harrison, and Alanson Sample. 2018. Wall++: Room-scale interactive and context-aware sensing. ACM, 273.
- [67] Chen Zhao, Sam Yisrael, Joshua R. Smith, and Shwetak N. Patel. 2014. Powering wireless sensor nodes with ambient temperature changes. ACM, 383–387.
- [68] Yinhua Zhou, Hyeunseok Cheun, Seungkeun Choi, William J. Potscavage Jr, Canek Fuentes-Hernandez, and Bernard Kippelen. 2010. Indium tin oxide-free and metal-free semitransparent organic solar cells. *Applied Physics Letters* 97, 15 (2010), 223.
- [69] Yinhua Zhou, Talha M. Khan, Jae Won Shim, Amir Dindar, Canek Fuentes-Hernandez, and Bernard Kippelen. 2014. All-plastic solar cells with a high photovoltaic dynamic range. *Journal of Materials Chemistry A* 2, 10 (2014), 3492–3497.